JNeurosci
THE JOURNAL OF NEUROSCIENCE

Research Articles: Neurobiology of Disease

Interferon-β plays a detrimental role in experimental traumatic brain injury by enhancing neuroinflammation that drives chronic neurodegeneration

https://doi.org/10.1523/JNEUROSCI.2516-19.2020

Cite as: J. Neurosci 2020; 10.1523/JNEUROSCI.2516-19.2020

Received: 22 October 2019
Revised: 22 January 2020
Accepted: 25 January 2020

Interferon-β plays a detrimental role in experimental traumatic brain injury by enhancing neuroinflammation that drives chronic neurodegeneration

James P. Barrett[1]*, Rebecca J. Henry[1], Kari Ann Shirey[2], Sarah J. Doran[1], Oleg D. Makarevich[1], Rodney R. Ritzel[1], Victoria A. Meadows[1], Stefanie N Vogel[2], Alan I. Faden[1], Bogdan A. Stoica[1,3,4] and David J. Loane[1,5]

[1]Department of Anesthesiology and Shock, Trauma and Anesthesiology Research (STAR) Center, University of Maryland School of Medicine, Baltimore, MD, USA.

[2]Department of Microbiology and Immunology, University of Maryland, Baltimore (UMB), Baltimore, MD, USA.

[3]Division of Translational Radiation Sciences (DTRS), Department of Radiation Oncology, University of Maryland School of Medicine, Baltimore, MD, USA.

[4]VA Maryland Health Care System, Baltimore VA Medical Center, Baltimore MD

[5]School of Biochemistry and Immunology, Trinity Biomedical Sciences institute, TCD, Ireland.

*Address correspondence to: James P. Barrett PhD, Department of Anesthesiology, University of Maryland School of Medicine, 655 West Baltimore Street, #6-011, Baltimore, MD 21201. Tel: 410-706-5188. E-mail: james.barrett@som.umaryland.edu

Short title: Inhibition of Interferon-β is protective following TBI

Number of pages: 39; Number of figures: 8

Number of words: Abstract (253), Introduction (604) and discussion (1550)

Key Words: Traumatic Brain Injury, Inflammation, IFN-β, Type I Interferons, Neurodegeneration

Conflict of interest statement: The other authors declare no competing interests.

Acknowledgements: This work was supported by National Institutes of Health grants R01NS082308 (D.J.L), R01NS037313 (A.I.F), R01NS096002 (B.A.S), R01NS110756 (D.J.L./A.I.F/B.A.S), AI125215 (S.N.V), U.S. Veterans Affairs grant 1I01 RX001993 (B.A.S), and Science Foundation Ireland grant 17/FRL/4860 (D.J.L).

Abstract

DNA damage and type I Interferons (IFNs) contribute to inflammatory responses after traumatic brain injury (TBI). TBI-induced activation of microglia and peripherally-derived inflammatory macrophages may lead to tissue damage and neurological deficits. Here, we investigated the role of interferon (IFN)-β in secondary injury after TBI using a controlled cortical impact model in adult male IFN-β-deficient (IFN-$\beta^{-/-}$) mice and assessed post-traumatic neuroinflammatory responses, neuropathology, and long-term functional recovery. TBI increased expression of DNA sensors cyclic GMP-AMP synthase (cGAS) and Stimulator of Interferon Genes (STING) in wildtype (WT) mice. IFN-β and other IFN-related and neuroinflammatory genes were also upregulated early and persistently after TBI. TBI increased expression of pro-inflammatory mediators in the cortex and hippocampus of WT mice, whereas levels were mitigated in IFN-$\beta^{-/-}$ mice. Moreover, long-term microglia activation, motor and cognitive function impairments were decreased in IFN-$\beta^{-/-}$ TBI mice compared to their injured WT counterparts; improved neurological recovery was associated with reduced lesion volume and hippocampal neurodegeneration in IFN-$\beta^{-/-}$ mice. Continuous central administration of a neutralizing antibody to the IFN-α/β receptor (IFNAR) for 3 days, beginning 30 minutes post-injury, reversed early cognitive impairments in TBI mice and led to transient improvements in motor function. However, anti-IFNAR treatment did not improve long-term functional recovery or decrease TBI neuropathology at 28 days post-injury. In summary, TBI induces a robust neuroinflammatory response that is associated with increased expression of IFN-β and other IFN-related genes. Inhibition of IFN-β reduces post-traumatic neuroinflammation and neurodegeneration, resulting in improved neurological recovery. Thus, IFN-β may be a potential therapeutic target for TBI.

53

54 **Significance Statement**

55 TBI frequently causes long-term neurological and psychiatric changes in head injury patients.
56 TBI-induced secondary injury processes including persistent neuroinflammation evolve over
57 time and can contribute to chronic neurological impairments. The present study demonstrates
58 that TBI is followed by robust activation of type I IFN pathways, which have been implicated in
59 microglial-associated neuroinflammation and chronic neurodegeneration. We examined the
60 effects of genetic or pharmacological inhibition of IFN-β, a key component of type I IFN
61 mechanisms to address its role in TBI pathophysiology. Inhibition of IFN-β signaling resulted in
62 reduced neuroinflammation, attenuated neurobehavioral deficits, and limited tissue loss long
63 after TBI. These pre-clinical findings suggest that IFN-β may be a potential therapeutic target
64 for TBI.

65

Introduction

Traumatic brain injury (TBI) is the leading cause of morbidity and mortality in developed countries (Maas et al. 2017). TBI induces delayed, secondary molecular and cellular injury responses, including chronic neuroinflammation, which contribute to progressive tissue loss and neurological impairments (Loane et al. 2014; Pischiutta et al. 2018). Clinical studies have shown that TBI induces chronic neurodegeneration that is associated with cognitive impairments and late-onset dementias (Mortimer et al. 1985; Plassman et al. 2000; Salib and Hillier 1997). In addition, experimental models of repeated mild or moderate-to-severe TBI result in persistent brain inflammation and neurodegeneration leading to long-term motor and cognitive function deficits (Loane et al. 2014; Aungst et al. 2014; Dixon et al. 1999; Mouzon et al. 2014; Pierce et al. 1998). Microglia, the primary innate immune cells in brain, are chronically activated for months to years following moderate-to-severe TBI in humans and in animal models (Johnson et al. 2013; Ramlackhansingh et al. 2011; Smith et al. 2013; Loane et al. 2014). Experimental evidence demonstrates that selected, delayed anti-inflammatory therapies reduce post-traumatic microglial activation and mitigate behavioral deficits and tissue loss after TBI (Byrnes et al. 2012; Piao et al. 2013).

Detection of nucleic acids by the innate immune system is essential for the host response during a viral infection. A number of immune sensors capable of recognizing cytosolic DNA have been identified, including the PHYIN family members AIM2, IFI16 (mouse homolog IFI204), and the enzyme cyclic GMP-AMP Synthase (cGAS). Activation of cGAS leads to activation of Stimulator of Interferon Genes (STING) and the induction of type I interferons (IFNs) (Almine et al. 2017). Type I IFNs are the main regulators of the host anti-viral response; in the absence of IFN signaling, mice are more susceptible to viral infection (Muller et al. 1994; Pinto et al. 2014). Following central nervous system (CNS) injury, damage associated molecular patterns, such as cytosolic and mitochondrial DNA, are released from injured neurons and initiate innate immune signaling that activates glia and drives secondary neuroinflammation

92 (Chin 2019; Walko et al. 2014; Wang et al. 2019). Microglia and astrocytes express members
93 of the PHYIN family, which are upregulated during neurodegenerative disease (Cox et al. 2015).
94 Inhibition of STING signaling reduces neuroinflammation and neurodegeneration in an
95 experimental model of prion disease (Nazmi et al. 2019). In addition, type I IFNs contribute to
96 the inflammatory response during normal aging and in age-related neurodegenerative disorders
97 (Baruch et al. 2014; Taylor et al. 2014; Roy et al. 2020). However, the role of type I IFNs within
98 the CNS is model-dependent; whereas IFNs in neurodegenerative models appear to be
99 detrimental (Taylor et al. 2014), IFN-β ameliorates neuroinflammatory responses in Multiple
100 Sclerosis (MS) (Owens et al. 2014; Prinz et al. 2008), possibly by reducing production of IL-12
101 (Byrnes, McArthur, and Karp 2002), and is the first disease-modifying drug approved for
102 relapsing-remitting MS (Paty and Li 1993; Jacobs et al. 2000).

103 Although several studies have implicated type I IFNs in models of age-related
104 neurodegeneration, the role of type I IFNs following CNS injury is poorly understood. One study
105 reported that inhibition of type I IFN signaling is protective during the acute phase after TBI
106 (Karve et al. 2016). However, their role in development of chronic neurological deficits and
107 progressive neurodegeneration following TBI has not been studied. Work in prion models
108 indicate that neurodegeneration is IFN-dependent, with peripheral inflammation further
109 increasing IFN-related gene expression and exacerbating disease progression (Field et al.
110 2010; Nazmi et al. 2019). Given this recent evidence, we examined the role of IFN-β in the
111 development of neuroinflammation, chronic neurodegeneration, and neurological impairments in
112 a well-characterized rodent TBI model, using genetic and pharmacological approaches.
113

Material and Methods

Animals: Studies were performed using adult male (10-12-week-old) IFN-β-deficient (IFN-$\beta^{-/-}$; provided by Stefanie Vogel, UMB, Baltimore, MD, Maryland), or age-matched C57BL/6J (WT) male mice (Jackson Laboratories, Bar Harbor, ME). IFN-$\beta^{-/-}$ mice have a targeted mutation in the gene that encodes IFN-β (Deonarain et al. 2003). IFN-$\beta^{-/-}$ mice were originally obtained from Dr. Eleanor Fish (University of Toronto) and were backcrossed to approximately N = 10 to C57BL/6J mice. Mice were housed in the Animal Care facility at the University of Maryland School of Medicine under a 12 h light-dark cycle, with *ad libitum* access to food and water. All surgical procedures were carried out in accordance with protocols approved by the Institutional Animal Care and Use Committee (IACUC) at the University of Maryland School of Medicine.

Controlled cortical impact (CCI): Our custom-designed CCI device consists of a microprocessor-controlled pneumatic impactor with a 3.5 mm diameter tip as described (Loane et al. 2009). Briefly, mice were anesthetized with isoflurane evaporated in a gas mixture containing 70% N_2O and 30% O_2 administered through a nose mask. Mice were placed on a heated pad and core body temperature was maintained at 37°C. The head was mounted in a stereotaxic frame, a 10-mm midline incision was made over the skull and the skin and fascia were reflected. A 5-mm craniotomy was made on the central aspect of the left parietal bone. The impounder tip of the injury device was then extended to its full stroke distance (44 mm), positioned to the surface of the exposed dura, and reset to impact the cortical surface. Moderate-level CCI was induced using an impactor velocity of 6 m/s and deformation depth of 2 mm. After injury, the incision was closed with interrupted 6-0 silk sutures, anesthesia was terminated, and the animal was placed into a heated cage to maintain normal core temperature for 45 minutes post-injury. Sham animals underwent the same procedure as CCI mice except for the impact.

Intracerebroventricular (i.c.v.) guide cannula implantation and osmotic pump infusion: Prior to CCI, the right lateral ventricle of the mouse was stereotaxically perforated with a brain

infusion kit 3 (ALZET, DURET Corporation, Cupertino, CA, USA; coordinates: 0.7 mm posterior to the bregma, 1.5 mm lateral to the bregma, 2 mm deep). Immediately following CCI on the left parietal cortex, the infusion cannula was connected to an osmotic minipump (ALZET; pump model: 1007D) that was implanted subcutaneously (s.c.) in the animal's back, just behind the scapula. Osmotic pumps were primed for approximately 8 h prior to implantation and were either filled with 0.5 mg/ml αIFNAR neutralizing antibody (MAR1-5A3; Invitrogen, USA) or an equal concentration isotype control mouse IgG1 (clone Mg1-45; Biolegend, San Diego, CA). Once implanted, the pumps continually infused αIFNAR or control IgG1 into the lateral ventricle for 3 days at a rate of 0.5 μL/h.

Study 1: WT sham-injured or CCI mice (n=5-6) were anesthetized (100 mg/kg sodium pentobarbital, I.P.) at 3 post-injury (dpi). Mice were transcardially perfused with ice-cold 0.9% saline (100 ml). Ipsilateral cortical and hippocampal tissue were rapidly dissected and snap-frozen on liquid nitrogen for RNA or protein extraction. An additional group of WT sham-injured or CCI mice (n=7) were anesthetized (100 mg/kg sodium pentobarbital, I.P.) at 60 dpi, ipsilateral cortical tissue was rapidly dissected and snap-frozen on liquid nitrogen for RNA extraction.

Study 2: WT and IFN-$\beta^{-/-}$ sham-injured (n=6) or CCI (n=6) of mice were anesthetized (100 mg/kg sodium pentobarbital, I.P.) at 3 days post-injury (dpi) and transcardially perfused with ice-cold 0.9% saline (100 ml). Ipsilateral cortical and hippocampal tissue were rapidly dissected and snap-frozen on liquid nitrogen for RNA and protein extraction.

Study 3: WT and IFN-$\beta^{-/-}$ sham-injured or CCI (n=8-15) mice were anesthetized (100 mg/kg sodium pentobarbital, I.P.). All animals underwent motor function testing (beam walk) on 1, 3, 7, 14, 21 and 28 dpi (Henry et al. 2019). Cognitive function was assessed using the Y-maze (8 dpi) (Henry et al. 2019) and the Novel Object Recognition test (NOR; 18 dpi) (Piao et al. 2013). At 28 dpi animals were anesthetized (100 mg/kg sodium pentobarbital, I.P.) and transcardially perfused with ice-cold 0.9% saline (100 ml), followed by 300 ml of 4% paraformaldehyde.

Brains were removed and post-fixed in 4% paraformaldehyde overnight, and cryoprotected in 30% sucrose for histological analysis.

Study 4: Antibody to the type I IFN receptor (αIFNAR; 0.5 mg/ml) or isotype control IgG1 was delivered i.c.v. via osmotic pump infusion to WT CCI mice (n=7-9/group). The dose of αIFNAR was chosen based on prior studies demonstrating neutralization of type I IFN in a mouse model of aging (Baruch et al. 2014). Sham WT mice (n=6) were used as control. All animals underwent motor function testing (beam walk) on 1, 3, 7, 14, 21 and 28 dpi, and cognitive function was assessed using the Y-maze (8 dpi) and Novel Object Recognition test (NOR; 18 dpi). At 28 dpi animals were anesthetized (100 mg/kg sodium pentobarbital, I.P.) and transcardially perfused with ice-cold 0.9% saline (100ml), followed by 300 ml of 4% paraformaldehyde. Brains were removed and post-fixed in 4% paraformaldehyde overnight, and cryoprotected in 30% sucrose for histological analysis.

Quantitative Real-time PCR (qRT-PCR): Total RNA was extracted from snap-frozen sham and TBI cortical tissue from WT and IFN-$\beta^{-/-}$ mice using an RNeasy isolation kit (Qiagen, Valencia, CA) with on-column DNase treatment (Qiagen). cDNA synthesis was performed using a Verso cDNA RT kit (Thermo Scientific, Pittsburg, PA) according to the manufacturer's instructions. qRT-PCR was performed using TaqMan gene expression assays (IFN-β, Mm00439552_s1; IRF1, Mm01288580_m1; IRF3, Mm00516784_m1; IRF4, Mm00516431_m1; IRF5, Mm00496477_m1; IRF7, Mm00516793_g1; ISG15, Mm01705338_s1; Mx1, Mm00487796_m1; IFI204, Mm00492602_m1; NOX2, Mm01287743_m1; TNFα, Mm00443258_m1; IL-6, Mm00446190_m1; IL-1ß, Mm01336189_m1; CCL5, Mm01302427_m1; CXCL10, Mm00445235_m1; ITGAM (CD11b), Mm00434455_m1; GFAP, Mm01253033_m1; Ym1, Mm00657889_m1; Arg1, Mm00475988_m1; SOCS3, Mm00545913_s1; IL-4Rα, Mm00446186_m1; TGF-β, Mm00441724_m1; and GAPDH, Mm99999915_g1; Applied Biosystems, Carlsbad, CA) on an ABI 7900 HT FAST Real Time PCR machine (Applied Biosystems). Samples were assayed in duplicate in one run (40 cycles), composed of 3 stages:

50°C for 2 min, 95°C for 10 sec for each cycle (denaturation), and finally the transcription step at 60°C for 1 min. Gene expression was calculated relative to the endogenous control sample (GAPDH) to determine relative expression values, using the 2−ΔΔCt method (where Ct is the threshold cycle) (Livak and Schmittgen 2001).

Western blot analysis: Proteins from ipsilateral cortical and hippocampal tissue were extracted using RIPA buffer, equalized, and loaded onto 5–20% gradient gels for SDS PAGE (Bio-Rad; Hercules, CA). Proteins were transferred onto nitrocellulose membranes, and then blocked for 1 h in 5 % milk in 1 × TBS containing 0.05 % Tween-20 (TBS-T) at room temperature. The membrane was incubated in rabbit anti-cGAS (1:1000; Cell signaling Danvers, MA), rabbit anti-STING (1:500; Cell signaling), rabbit anti-STAT1 (1:1000; Cell signaling) or mouse anti-β-Actin (1:5000; Sigma-Alrich) overnight at 4°C, then washed three times in TBS-T, and incubated in appropriate HRP-conjugated secondary antibodies (Jackson ImmunoResearch Laboratories, West Grove, PA) for 2 h at room temperature. Membranes were washed three times in TBS-T, and proteins were visualized using SuperSignal West Dura Extended Duration Substrate (Thermo Scientific, Rockford, IL). Chemiluminescence was captured ChemiDoc™ XRS+ System (Bio-Rad), and protein bands were quantified by densitometric analysis using BioRad Molecular Imaging Software. The data presented reflects the intensity of target protein band normalized to the intensity of the endogenous control for each sample (expressed in arbitrary units).

Immunofluorescence Imaging: Coronal brain sections from sham and CCI mice at ~ −1.70 mm from the bregma were selected, and standard immunostaining techniques were employed (Henry et al. 2019). Briefly, 20-µm brain sections were washed 3 times with 1× PBS, blocked for 1 h in goat serum containing 0.4% Triton X-100, and incubated overnight at 4 °C with a combination of primary antibodies, including mouse anti-gp91^{phox} (NOX2, 1:1000; BD Biosciences) and rat anti-CD68 (1:1000; AbD Serotec, Inc., Raleigh, NC). Sections were washed 3 times with 1× PBS and incubated with appropriate Alexa Fluor-conjugated secondary

antibodies (Life Technologies) for 2 h at room temperature. Sections were washed 3 times with 1× PBS, counterstained with 4′,6-diamidino-2-phenylindole (DAPI; 1 µg/ml; Sigma, Dorset, UK), and mounted with glass coverslips using hydromount solution (NationalDiagnostics, Atlanta,GA). Images were acquired using a fluorescent Nikon Ti-E inverted microscope (Nikon Instrument, Inc., Melville, NY), at 10 × (Plan Apo 10× NA 0.45) or 20 × (Plan APO 20× NA 0.75) magnification. Exposure times were kept constant for all sections in each experiment. All images were quantified using Nikon ND-Elements software (AR 4.20.01). Analysis was performed via Nikon's NIS-Elements software to identify nuclei count (DAPI), CD68+ and NOX2+ cells on the best focused image per region (automatically determined via software). For quantification, the total signal intensity of NOX2 within CD68+ regions was summed across each field and normalized to the nuclear count per field. The normalized sum intensity data from at least three fields was averaged for each animal.

Stereology:

Lesion volume: Sixty µm coronal sections from mice were stained with cresyl violet (FD NeuroTechnologies, Baltimore, MD), dehydrated, and mounted for analysis. Lesion volume was quantified based on the Cavalieri method of unbiased stereology using Stereoinvestigator Software (MBF Biosciences, Williston, VT) as described (Kumar et al. 2013). Briefly, lesion volume was quantified by outlining the missing tissue on the injured hemisphere using the Cavalieri estimator with a grid spacing of 0.1 mm. Every 8^{th} section from a total of 96 sections was analyzed beginning from a random start point.

Neuronal cell loss: Cresyl violet stained 60 µm coronal sections were used to quantify neuronal densities in the dentate gyrus region of the hippocampus of both sham and CCI mice. The optical fractionator method of stereology was employed as previously described (Kumar et al. 2016). Briefly, every fourth 60 µm section between -1.22 and -2.54 mm from bregma was analyzed beginning from a random start point. A total of 5 sections were analyzed. The optical

dissector had a size of 50 x 50 µm in the x-axis and the y-axis, respectively, with a height of 10 µm and a guard zone of 4 µm from the top of the section. The sampled regions of the dentate gyrus was demarcated in the injured hemisphere and cresyl violet-positive cells were counted using Stereoinvestigator Software (MBF Biosciences). The volume of the dentate gyrus was measured using the Cavalieri estimator method with a grid spacing of 50 µm. The number of surviving neurons in each field was divided by the volume of the region of interest to obtain the cellular density expressed in counts/mm^3.

Neurobehavioral testing:

Beam walk: Motor function recovery was assessed using a beam walk test as described (Loane et al. 2009). The beam walk tests fine motor coordination differences and consists of a narrow wooden beam (5 mm wide and 120 mm in length), which is suspended 300 mm above a tabletop. Mice were placed on one end of the beam, and the number of foot faults of the right hind limb recorded over 50 steps. Mice were trained on the beam walk for 3 days prior to CCI and tested through 28 dpi.

Y-maze spontaneous alternation: The Y-maze test assesses spatial working memory and was performed as previously described (Kumar et al. 2016). Briefly, the Y-maze (Stoelting Co., Wood Dale, IL) consisted of three identical arms, each arm 35 cm long, 5 cm wide, and 10 cm high, at an angle of 120° with respect to the other arms. One arm was randomly selected as the "start" arm, and the mouse was placed within and allowed to explore the maze freely for 5 min. Arm entries (arms A–C) were recorded by analyzing mouse activity using ANY-maze software (Stoelting Co., Wood Dale, IL). An arm entry was attributed when all four paws of the mouse entered the arm, and an alternation was designated when the mouse entered three different arms consecutively. The percentage of alternation was calculated as follows: total alternations x 100/(total arm entries − 2). If a mouse scored >50% alternations (the chance level for choosing the unfamiliar arm), this was indicative of spatial working memory.

Novel object recognition (NOR): NOR was performed on 17-18 dpi to assess non-spatial hippocampal-mediated memory, as previously described (Piao et al. 2013). Mice were placed in an open field (22.5 cm X 22.5 cm) and two identical objects were placed near the left and right corners of the open field for training (familiar phase). Mice were allowed to freely explore until they spent a total of 20 sec exploring the objects (exploration was recorded when the front paws or nose contacted the object). The time spent with each object was recorded using Any-Maze software (Stoelting Co.). After 24 h, object recognition was tested by substituting a novel object for a familiar training object (the novel object location was counterbalanced across mice). Because mice inherently prefer to explore novel objects, a preference for the novel object (more time than chance [15 sec] spent with the novel object) indicates intact memory for the familiar object.

Statistical analysis: Mice that were ear tagged and housed five per cage were randomly removed one at a time from the cage and assigned to groups until sufficient numbers were reached for each group. Blinding was performed as follows: a) individual who administered drugs was blinded to treatment group, and b) behavioral and stereological analyses were performed by individuals blinded to injury or treatment groups. Quantitative data were expressed as mean ± standard errors of the mean (s.e.m.). Normality testing was performed and data sets passed normality (D'Agostino & Pearson omnibus normality test), and therefore parametric statistical analysis was performed. Statistical analysis was carried out using a two-way analysis of variance (ANOVA) with Tukey *post-hoc* tests, or one-way ANOVA followed by Tukey *post-hoc* analysis to identify differences between groups. When comparisons were made between two conditions, an unpaired Student's *t* test was performed. Statistical analyses were performed using GraphPad Prism Program, Version 8 for Windows (GraphPad Software, San Diego, CA, USA). Significance level was set as $p<0.05$.

Results

3.1. TBI results in the activation of cGAS/STING pathway and the induction of type I IFN responses in the injured cortex and hippocampus.

Ipsilateral cortical and hippocampal tissue were collected at 72 hours after moderate-level CCI for expression analysis of IFN-β and IFN-stimulated genes (ISGs). Activation of cGAS and STING induces the production of type I IFNs (Cheng et al. 2018; Almine et al. 2017). Therefore, we evaluated the cortical expression of cGAS and STING by Western blot (**Fig.1A**) and demonstrated that TBI increased protein expression of cGAS ($t_{(8)}$=4.395, p=0.0023 *vs*. sham, *t* test; **Fig.1B**) and STING ($t_{(8)}$=6.202, p=0.0003 *vs*. sham; **Fig.1C**). In addition, IFN-β mRNA expression was also increased in the cortex at 72 hours post-injury ($t_{(8)}$=3.885, p=0.006 *vs.* sham; **Fig.1D**). We next examined upregulation of genes required for downstream signaling pathways. STAT1 is a mediator of type I IFN-mediated responses (Ivashkiv and Donlin 2014). STAT1 protein was increased in the cortex of TBI mice ($t_{(8)}$=3.442, p=0.0088 *vs*. sham; **Fig.1E**). We also evaluated Interferon Regulatory Factors (IRFs), transcription factors that induce type I IFNs (IRF3, IRF7) and propagate type I IFN responses (IRF1, IRF4 and IRF5) (Honda, Takaoka, and Taniguchi 2006; Lazear et al. 2013; Gunthner and Anders 2013). TBI increased mRNA expression of IRF3 ($t_{(8)}$=7.064, p=0.0002 *vs*. sham; **Fig.1F**) , IRF1 ($t_{(8)}$=5.047, p=0.002 *vs*. sham; **Fig.1G**), IRF4 ($t_{(8)}$=3.165, p=0.016 *vs*. sham; **Fig.1H**), IRF5 ($t_{(8)}$=6.935, p=0.0002 *vs*. sham; **Fig.1I**) and IRF7 ($t_{(8)}$=2.417, p=0.046 *vs*. sham; **Fig.1J**). Similar protein and mRNA expression patterns were observed in the ipsilateral hippocampus at 72 hours post-injury (**Fig.1K-T**).

3.2. IFN-β deficiency attenuates type I IFN signature in the brain following TBI

Having demonstrated a type I IFN signature in the cortex and hippocampus following TBI, we investigated the possible role of IFN-β on the inflammatory response after TBI, using mice with a targeted mutation in IFN-β (designated IFN-$\beta^{-/-}$). At 72 hours post-injury, TBI

increased cGAS ($F_{(1,19)}$=43.71, p<0.0001; two-way ANOVA; **Fig.2B**) and STING ($F_{(1,19)}$=32.15; p<0.0001; **Fig.2C**) protein expression comparably in both WT and IFN-$\beta^{-/-}$ mice compared to sham operated counterparts. TBI also increased STAT1 protein expression in the cortex of WT mice ($F_{(1,19)}$=16.06, p=0.0008; **Fig.2D**), but levels were reduced in IFN-$\beta^{-/-}$ mice. There was a significant effect of genotype ($F_{(1,19)}$=8.866, p=0.0077), and post-hoc analysis demonstrated a significant reduction in STAT1 protein expression in IFN-$\beta^{-/-}$ TBI mice (p=0.024, WT TBI vs IFN-$\beta^{-/-}$TBI).

We next assessed IRF expression patterns in WT and IFN-$\beta^{-/-}$ mice. TBI significantly increased mRNA expression of IRF1 ($F_{(1,19)}$=108.1, p<0.0001; **Fig.2E**), IRF3 ($F_{(1,19)}$=4.4, p=0.0478; **Fig.2F**), IRF4 ($F_{(1,19)}$=6.3, p=0.0208; **Fig.2G**), IRF5 ($F_{(1,19)}$=42.5, p<0.0001; **Fig.2H**), and IRF7 ($F_{(1,19)}$=73.45, p<0.0001; **Fig.2I**). While the TBI-induced increase in the expression of IRF3, IRF4 and IRF5 was comparable in WT and IFN-$\beta^{-/-}$ mice, there was a significant effect of genotype on IRF1 ($F_{(1,19)}$=12.5, p=0.0025) and IRF7 ($F_{(1,19)}$=72.82, p<0.0001) mRNA expression, as well as a significant interaction between TBI and genotype (IRF1, $F_{(1,19)}$=8.274, p=0.0097; IRF7, $F_{(1,19)}$=54.58, p<0.0001). Post-hoc analysis demonstrated that IRF1 and IRF7 mRNA expression was significantly decreased in IFN-$\beta^{-/-}$ TBI mice (IRF1 [p=0.0016], IRF7 [p<0.0001], WT TBI *vs*. IFN-$\beta^{-/-}$ TBI). We then examined mRNA expression of genes associated with IFN-mediated antiviral responses, including ISG15, MX1, and IFI204. TBI increased mRNA expression of ISG15 ($F_{(1,19)}$=17.78, p=0.0005; **Fig.2J**), MX1 ($F_{(1,19)}$=102.1, p<0.0001; **Fig.2K**) and IFI204 ($F_{(1,19)}$=126.0, p<0.0001; **Fig.2L**) in the cortex of WT TBI mice, but not IFN-β TBI mice. There was a significant genotype effect on all genes (ISG15 ($F_{(1,19)}$=32.07, p<0.0001), MX1 ($F_{(1,19)}$=93.98, p<0.0001) and IFI204 ($F_{(1,19)}$=66.29, p<0.0001)), and an interaction between TBI and genotype for ISG15 ($F_{(1,19)}$=12.06, p=0.0025), MX1 ($F_{(1,19)}$=79.23, p<0.0001) and IFI204 ($F_{(1,19)}$=63.07, p<0.0001). Post-hoc analysis revealed that ISG15, MX1, IFI204 mRNA

expression was significantly decreased in IFN-$\beta^{-/-}$ TBI mice (ISG15, $p<0.0001$; MX1, $p<0.0001$; and IFI204, $p<0.0001$; WT TBI *vs*. IFN-$\beta^{-/-}$ TBI).

In the hippocampus, cGAS and STING protein expression were also increased in WT TBI mice at 72 hours post-injury (cGAS, $F_{(1,16)}=43.07$, $p<0.0001$ (**Fig.2M**); STING, $F_{(1,16)}=35.66$, $p<0.0001$; (**Fig.2N**)). In contrast to the cortex, however, there was a significant genotype effect (cGAS, $F_{(1,16)}=12.52$, $p=0.0027$; STING, $F_{(1,16)}=14.09$, $p=0.0017$) and a significant interaction between TBI and genotype (cGAS, $F_{(1,16)}=13.01$, $p=0.0024$; STING, $F_{(1,16)}=14{,}47$ $p=0.0016$). Hippocampal cGAS and STING protein expression was significantly decreased in IFN-$\beta^{-/-}$ TBI mice (cGAS, $p=0.0007$, STING, $p=0.0004$, WT TBI *vs*. IFN-$\beta^{-/-}$ TBI). Similarly, TBI-induced STAT1 protein expression was attenuated in IFN-$\beta^{-/-}$ TBI mice (**Fig.2O**). There were main effects of TBI ($F_{(1,16)}=14.82$, $p=0.0014$), and genotype ($F_{(1,16)}=12.95$, $p=0.0024$), but no significant interactions between them. Post-hoc analysis demonstrated that hippocampal STAT1 protein expression was significantly reduced in IFN$\beta^{-/-}$ TBI mice ($p=0.0073$, WT TBI *vs*. IFN-$\beta^{-/-}$ TBI). Furthermore, TBI increased hippocampal mRNA expression of IRF7 ($F_{(1,16)}=14.66$, $p=0.0015$; **Fig.2P**), ISG15 ($F_{(1,16)}=11.77$, $p=0.0034$; **Fig.2R**), MX1 ($F_{(1,16)}=26.01$, $p=0.0001$; **Fig.2S**) and IFI204 ($F_{(1,16)}=10.48$, $p=0.0052$; **Fig.2T**) in WT mice. There was a significant genotype effect on all genes (IRF7 ($F_{(1,16)}=17.05$, $p=0.0008$), ISG15 ($F_{(1,16)}=12.61$, $p=0.0027$), MX1 ($F_{(1,19)}=21.99$, $p=0.0002$) and IFI204 ($F_{(1,16)}=7.187$, $p=0.0164$)), and a significant interaction between TBI and genotype (IRF7 ($F_{(1,16)}=13.80$, $p=0.0019$), ISG15 ($F_{(1,16)}=13.69$, $p=0.0019$), MX1 ($F_{(1,16)}=21.18$, $p=0.0003$) and IFI204 ($F_{(1,16)}=7.195$, $p=0.0164$). Post-hoc analysis revealed that hippocampal IRF7, ISG15, MX1, and IFI204 mRNA expression was significantly reduced in IFN$\beta^{-/-}$ TBI mice (IRF7, $p=0.0002$; ISG15, $p=0.0006$; MX1, $p<0.0001$; and IFI204, $p=0.0078$; WT TBI vs IFN-$\beta^{-/-}$ TBI). Overall, these data demonstrate that IFN-β plays an important role in the development of the type I IFN gene signature in the cortex and hippocampus acutely after TBI.

3.3. IFN-β deficiency results in an altered inflammatory response following TBI

We next examined classical neuroinflammatory responses following TBI. Cortical expression of pro-inflammatory genes, TNF-α, NOX2, IL-6, IL-1β, CCL5, CXCL10, and markers of glial activation, ITGAM (CD11b, for microglia) and GFAP (for astrocytes), were assessed in WT and IFN-$\beta^{-/-}$ mice at 72 hours post-injury. TBI induced a robust increase in the mRNA expression of TNF-α ($F_{(1,19)}$=72.63, p<0.0001; **Fig.3A**), NOX2 ($F_{(1,19)}$=48.53, p<0.0001; **Fig.3B**), IL-6 ($F_{(1,19)}$=14.01, p=0.0014; **Fig.3C**), IL-1β ($F_{(1,19)}$=36.13, p<0.0001; **Fig.3D**), CCL5 ($F_{(1,19)}$=266.7, p<0.0001; **Fig.3E**), CXCL10 ($F_{(1,19)}$=29.99, p<0.0001; **Fig.3F**), ITGAM ($F_{(1,19)}$=159.3, p<0.0001; **Fig.3G**), and GFAP ($F_{(1,19)}$=286.2, p<0.0001; ANOVA; **Fig.3H**). There was a significant genotype effect on TNF-α ($F_{(1,19)}$=6.355, p=0.0208), NOX2 ($F_{(1,19)}$=8.937, p=0.0075), CCL5 ($F_{(1,19)}$=27.37, p<0.0001), and CXCL10 ($F_{(1,19)}$=24.73, p<0.0001), and a significant interaction of TBI and genotype for all genes (TNF-α ($F_{(1,19)}$=6.121, p=0.0230), NOX2 ($F_{(1,19)}$=9.189, p=0.0069), CCL5 ($F_{(1,19)}$=28.72, p<0.0001) and CXCL10 ($F_{(1,19)}$=23.36, p<0.0001)). Post-hoc analysis demonstrated a significant reduction in TNF-α, NOX2, CCL5 and CXCL10 mRNA expression in IFN-$\beta^{-/-}$ TBI mice (TNF-α, p=0.0131; NOX2, p=0.0027; CCL5, p<0.0001; CXCL10, p<0.0001; WT TBI *vs*. IFN-$\beta^{-/-}$ TBI). Interestingly, both Itgam (CD11b) mRNA and GFAP mRNA were upregulated in WT and IFN-$\beta^{-/-}$ TBI mice to a comparable extent (**Fig.3G,H**). Similar effects of IFN-$\beta^{-/-}$ genotype on mRNA expression patterns of TNF-α, NOX2, CCL5 and CXCL10 were observed in the ipsilateral hippocampus at 72 hours post-injury (**Fig.3I-L**). Overall, our data suggest a role for IFN-β in the induction of classical pro-inflammatory response acutely after TBI.

Previously, we demonstrated that a decrease in the pro-inflammatory response after TBI concurrently resulted in increased expression of pro- and anti-inflammatory genes (Kumar et al. 2016; Barrett et al. 2017). Thus, we assessed the mRNA expression of genes associated with anti-inflammatory responses, such as Arg1, YM1, IL-10, SOCS3 and TGFβ, in the cortex at 72 hours post-injury. TBI increased cortical expression of Arg1 ($F_{(1,19)}$=21.73, p=0.0002; **Fig.4A**),

YM1 ($F_{(1,19)}$=56.16, p<0.0001; **Fig.4B**), IL-10 ($F_{(1,19)}$=60.13, p<0.0001; **Fig.4C**), SOCS3 ($F_{(1,19)}$=46.25, p<0.0001; **Fig.4D**) and TGFβ ($F_{(1,19)}$=131.7, p<0.0001; **Fig.4E**) in WT mice compared to sham mice. There was a genotype effect for YM1 ($F_{(1,16)}$=9.669, p=0.0058), and IL-10 ($F_{(1,16)}$=24.55, p<0.0001) only, and a significant interaction between TBI and genotype for YM1 ($F_{(1,16)}$=9.415, p=0.0063) and IL-10 ($F_{(1,16)}$=23.63, p=0.0001). YM1 and IL-10 mRNA expression was significantly reduced in the cortex of IFN-$\beta^{-/-}$ TBI mice (YM1, p=0.0022; IL-10, p<0.0001; WT TBI *vs.* IFN-$\beta^{-/-}$ TBI). Similar effects of IFN-$\beta^{-/-}$ genotype on mRNA expression patterns of Arg1, YM1, SOCS3, and TGFβ were observed in the ipsilateral hippocampus at 72 hours post-injury (**Fig.4F-I**). IL-10 mRNA expression was undetectable in the hippocampus of all animals.

3.4 IFN-β deficiency improves long-term motor and cognitive function recovery after TBI

To investigate the long-term consequences of IFN-β genetic deletion on TBI outcomes, we evaluated motor and cognitive recovery in sham and TBI WT and IFN-$\beta^{-/-}$ mice through 28 days post-injury (dpi). We performed a beam walk task to assess deficits in fine-motor coordination. TBI produced significant motor function impairments in WT TBI mice, with 50 ± 0 footfaults (FF) at 1 dpi and persistent footfaults through 28 dpi (47±1 FF; p<0.0001 *vs.* WT sham; RM-ANOVA, **Fig.5A**). In contrast, IFN-$\beta^{-/-}$ TBI mice exhibited improved motor performance with a reduced number of footfaults at 7 (32±2 FF; p<0.0001 *vs.* WT TBI), 14, (31±2 FF; p<0.0001 *vs.* WT TBI), 21, (31±3 FF; p<0.0001 *vs.* WT TBI) and 28 dpi (36±3 FF; p<0.0001 *vs.* WT TBI).

Hippocampal-dependent spatial working memory was also assessed using a Y-maze test at 8 dpi. TBI resulted in deficits in working memory in TBI mice ($F_{(1,38)}$=6.660, p=0.0137; Two-way ANOVA, **Fig. 5B**), but only WT TBI mice had significantly decreased spontaneous alternations (p=0.0151 *vs.* WT sham). Each group of mice had equivalent numbers of arm

418 entries in the Y-maze test. To assess hippocampal-dependent non-spatial learning, we used a
419 novel object recognition (NOR) test at 17 and 18 dpi. During the familiar phase of the test, there
420 was no difference between groups with regard to time spent with either the right or left objects,
421 indicating no side preference. Twenty-four hours later, mice were retested with a novel object.
422 Compared to WT sham mice (61.8 ± 1.8%), WT TBI mice spent less time with the novel object
423 (49.3 ± 1.7%; **Fig.5C**). In contrast, both IFN-$\beta^{-/-}$ sham and TBI mice spent an increased amount
424 of time with the novel object (62.2.0 ± 2.4% and 64.3 ± 1.8%, respectively; TBI effect,
425 $F_{(1,38)}$=16.48, p=0.0008; genotype effect, $F_{(1,38)}$=12.01, p=0.0013; interaction, $F_{(1,38)}$=8.464,
426 p=0.0060; WT TBI vs IFN-$\beta^{-/-}$ TBI comparison, adjusted p<0.0001, **Fig.5C**).
427
428 **3.5 IFN-β deficiency reduces microglial activation and neurodegeneration after TBI**
429 To assess the effects of IFN-β deficiency on post-traumatic neuroinflammation we
430 evaluated NOX2 expression in reactive microglia/macrophages (CD68+ cells) in the injured
431 cortex at 28 dpi. TBI induced robust NOX2 expression in CD68+ microglia/macrophages in the
432 cortex of WT and IFN-$\beta^{-/-}$ TBI mice ($F_{(1,10)}$=30.12, p=0.0003; two-way ANOVA; **Fig. 6A**). There
433 was a significant genotype effect ($F_{(1,10)}$=5.420, p=0.0422), and post-hoc analysis demonstrated
434 that IFN-β deficiency was associated with reduced NOX2 expression in the injured cortex
435 (p=0.0207 IFN-$\beta^{-/-}$ TBI *vs.* WT TBI).
436 In order to examine the effects of IFN-β deficiency on neurodegeneration, we examined
437 TBI-induced lesion volume and neuronal loss at 28 dpi. TBI-induced lesion volume was
438 significantly reduced in IFN-$\beta^{-/-}$ TBI mice (2.6±0.35 mm^3) when compared to WT TBI mice
439 (4.17±0.29 mm^3; $t_{(11)}$=3.399, p=0.003, t-test; *vs.* WT TBI; **Fig. 6B)**. Furthermore, TBI resulted in
440 hippocampal neurodegeneration with a significant loss of neurons in the dentate gyrus when
441 compared to sham WT mice ($F_{(1,15)}$=4.86, p=0.0435; two-way ANOVA; **Fig.6C**). There was a
442 significant genotype effect ($F_{(1,15)}$=22.53, p=0.0002) and an interaction of TBI and genotype

($F_{(1,15)}$=16.05, p=0.0011), with neuronal density being equivalent to sham levels in the IFN-$\beta^{-/-}$ TBI mice. Notably, hippocampal neuronal loss was reduced in IFN-$\beta^{-/-}$ TBI mice (932,580±32,045 cells/mm^3) compared to WT TBI mice (621,054±37,628 cells/mm^3; p=0.0001 *vs.* WT TBI). Overall, these data demonstrate that IFN-β deficiency results in improvements in long-term motor and cognitive function recovery and reduced NOX2-associated microglial activation and related neurodegeneration after TBI.

3.6 Central administration of neutralizing αIFNAR improves acute phase neurological function, but fails to improve long-term neurological recovery or reduce neurodegeneration after TBI

We next investigated whether post-injury treatment of TBI mice with a neutralizing type I IFN receptor antibody (αIFNAR) could improve functional recovery. The absence of drug-based interventions that can specifically target IFN-β limited our ability to mimic the genetic knockout. Because IFNAR is a shared IFN-α/β receptor, our treatment regime using αIFNAR inhibits more broad range type I IFN responses, with the advantage of potentially increasing therapeutic relevance. CCI mice received a central infusion of αIFNAR (12 μg/day) or an equal concentration of an isotype-matched control antibody (IgG1) via contralateral ICV administration using Alzet pumps, beginning at 30 minutes post-injury and continuing through 3 dpi. Motor and cognitive function recovery were assessed up to 28 dpi, and TBI neuropathology was also evaluated at 28 dpi.

When compared to sham mice, TBI resulted in fine-motor coordination deficits in IgG-treated TBI mice, with 50 ± 0 footfaults at 1 dpi that persisted through 28 dpi (42±2 FF; p<0.0001 *vs.* sham; RM-ANOVA; **Fig.7A**). Administration of αIFNAR significantly improved motor function recovery at 14 dpi (34±3 FF; p=0.0431 *vs.* TBI+IgG), although this improvement was not sustained. We also assessed hippocampal-dependent spatial working memory at 8 dpi

using a Y-maze test. TBI induced cognitive deficits in the Y-maze test ($F_{(2,18)}$=5.723; p=0.0119, ANOVA; **Fig.7B**), such that IgG-treated TBI mice had reduced spontaneous alternations (p=0.0245 *vs*. sham; **Fig.7B**). In contrast, αIFNAR-treated TBI mice exhibited increased spontaneous alternations (p=0.0282 *vs*. IgG-treated TBI mice; **Fig.7B**), and performed to similar level as sham mice in this cognitive task. Each group of mice had approximately equal numbers of arm entries in the Y-maze test.

We then assessed hippocampal-dependent non-spatial learning after TBI using NOR test at 17 and 18 dpi. During the familiar phase of the test, there was no difference between groups with regard to time spent with either the right or left objects, indicating no side preference. Twenty-four hours later, mice were retested with a novel object. Compared to WT sham mice (76.6 ± 2.3%; **Fig.7C**), IgG-treated and αIFNAR-treated TBI mice spent less time with the novel object (53.8 ± 2.8% and 57.5 ± 2.1%, respectively; **Fig.7C**). However, central administration of αIFNAR failed to improve working memory in this test (TBI effect, $F_{(2,18)}$=19.78, p<0.0001 IgG-treated TBI mice *vs.* sham; p=0.002 αIFNAR-treated TBI mice *vs.* sham). Finally, we quantified TBI-induced lesion volume in the ipsilateral cortex of IgG- and αIFNAR-treated TBI mice at 28 dpi. αIFNAR treatment failed to reduce TBI-induced lesion volume (3.6±0.69 mm^3) when compared to IgG-treated TBI mice (4.1±0.54 mm^3; **Fig.7D**).

3.7 Type I IFN genes are chronically elevated in the injured cortex following TBI

The failure of short-term αIFNAR neutralization to reduce chronic neurological impairments and neurodegeneration after TBI indicates that IFN-related pathways are active for prolonged periods after TBI. Therefore, we set out to assess their expression during the chronic phase of TBI. Ipsilateral cortical tissue was collected at 60 days post-injury to quantify the expression of ISGs and pro-inflammatory genes. We determined that key ISGs and pro-inflammatory genes remain significantly upregulated in the chronically injured cortex. While there was no effect of TBI on cGAS gene expression (**Fig. 8A**), we found that TBI increased

mRNA expression of STING ($t_{(12)}$=4.593, p=0.0006 *vs*. sham; **Fig.8B**) , STAT1 ($t_{(12)}$=3.929, p=0.0020 *vs*. sham; **Fig.8C**), IRF1 ($t_{(12)}$=3.197, p=0.0077 *vs*. sham; **Fig.8D)**, IRF7 ($t_{(12)}$=3.647, p=0.046 *vs*. sham; **Fig.8E**), CXCL10 ($t_{(12)}$=3.220, p=0.0074 *vs*. sham; **Fig.8F**), ISG15 ($t_{(12)}$=2.616, p=0.0225 *vs*. sham; **Fig.8G**) and IFI204 ($t_{(12)}$=5.132, p=0.0002 *vs*. sham; **Fig.8H**). Chronic TBI also increased mRNA expression of pro-inflammatory TNF-α ($t_{(12)}$=3.006, p=0.0101 *vs*. sham; **Fig.8I**), NOX2 ($t_{(12)}$=4.591, p=0.0005 *vs*. sham; **Fig.8J**), CCL5 ($t_{(12)}$=3.642, p=0.003 *vs*. sham; **Fig.8K**), and glial activation markers CD11b ($t_{(12)}$=5.867, p<0.0001 *vs*. sham; **Fig.8L**), CD68 ($t_{(12)}$=5.353, p=0.0001 *vs*. sham; **Fig.8M**), and GFAP ($t_{(12)}$=5..381, p=0.0001 *vs*. sham; **Fig.8N**).

Discussion

Prior pre-clinical studies have shown that IFNAR1 (IFN-α and -β receptor) knockout mice have reduced lesion size and pro-inflammatory cytokine expression as well as increased levels of anti-inflammatory mediators following TBI (Karve et al. 2016). This indicates that type I IFNs contribute to secondary neuroinflammation after TBI, and inhibiting these pathways will result in neuroprotection. However, studies based on IFNAR signaling cannot pinpoint the functional contribution of IFN-α and IFN-β during neuroprotection. Moreover, similar to its protective actions in MS (Scheu et al. 2019), exogenous administration of IFN-β following spinal cord injury improves functional recovery in mice, in part by reducing lipid peroxidation and inflammatory cytokines (Gok et al. 2007; Sandrow-Feinberg et al. 2010). This highlights the complex role of IFN-β during secondary injury and CNS repair. Here, our pre-clinical studies using IFN-β knockout mice demonstrate that IFN-β drives secondary neuroinflammation because genetic deletion of IFN-β results in improved motor and cognitive function recovery following TBI and reduces chronic neurodegeneration. As such, this is the first study to implicate IFN-β in the development of neurological dysfunction and neurodegeneration following TBI.

DNA released from dying cells can act as an alarmin, resulting in the activation of the immune response (Almine et al. 2017). We demonstrate that cGAS and STING, critical components of the cytosolic DNA sensing machinery, are robustly upregulated in the injured cortex and hippocampus within 72 hours of brain trauma. Others have shown that STING mRNA is induced immediately after TBI, and is associated with elevated expression of IFN-related and inflammatory genes (Abdullah et al. 2018). Activation of cGAS-STING pathway in our model was accompanied by a robust increase in IFN-β mRNA expression in the injured brain. While a recent study demonstrates that neurons under ER stress upregulate IFN-β after TBI (Sen et al. 2020), it is also likely that other cells, including glia (Cox et al. 2015), produce IFN-β during secondary neuroinflammation. Importantly, it has also been reported that IFN-β

529 mRNA is highly upregulated after 6 hours of TBI in human postmortem tissue, and specifically in
530 the injured hemisphere (Karve et al. 2016).

531 We also found that STAT1, a key mediator of type I IFN responses (Ivashkiv and Donlin
532 2014), was also upregulated in the injured brain. IRFs are involved in the induction and
533 amplification of type I IFN responses (Honda and Taniguchi 2006). IRF3 is required for the
534 production of IFN-β (Honda and Taniguchi 2006; Hatesuer et al. 2017; Akira, Uematsu, and
535 Takeuchi 2006), whereas IRF1 and IRF5 contribute to the propagation of pro-inflammatory
536 responses (Takaoka et al. 2005; Liu et al. 2003; Xie et al. 2016). Furthermore, IRF4 is involved
537 in the induction of anti-inflammatory cytokines, IL-4 and IL-10 (Ahyi et al. 2009), while IRF7
538 amplifies type I IFN responses, such that deletion of IRF7 diminishes responses to inflammatory
539 stimuli (Honda et al. 2005; Tanaka et al. 2015). We determined that IRF1, IRF3, IRF4, IRF5,
540 and IRF7 mRNA expression were significantly upregulated within 72 hours of brain trauma.
541 Notably, TBI-induced STAT1 expression was significantly reduced in IFN-$\beta^{-/-}$ TBI mice, as were
542 expression levels of IRF1 and IRF7 mRNA. The latter observation is in agreement with a
543 previous report that IRF7 mRNA expression was decreased in IFNAR1 knockout mice (Karve et
544 al. 2016). Interestingly, lipopolysaccharide-induced STAT1, IRF1, and IRF7 changes have been
545 shown to be reduced in IFN-$\beta^{-/-}$ macrophages compared to WT macrophages (Sheikh et al.
546 2014; Thomas et al. 2006). We also demonstrated that the TBI-related increase in viral
547 response genes (ISG15, MX1 and IFI204) was significantly reduced in IFN$\beta^{-/-}$ TBI mice.

548 Levels of pro-inflammatory cytokines and chemokines (TNF-α, NOX2, IL-6, CCL5,
549 CXCL10) were reduced in the injured cortex of IFN$\beta^{-/-}$ mice compared to their WT counterparts.
550 These findings support prior reports that decreased type I IFN signaling is associated with
551 decreased inflammatory gene expression during the acute phase after TBI (Abdullah et al.
552 2018; Karve et al. 2016). Inhibition of type I IFNs also reduce chronic neuroinflammation in
553 models of AD (Minter et al. 2016), Parkinson's disease (Main et al. 2016), and prion disease

554 (Nazmi et al. 2019). Although anti-inflammatory markers, Arg1, SOCS3 and TGFβ mRNA
555 expression levels were similar in the cortex WT and IFNβ$^{-/-}$ mice, the expression levels of the IL-
556 10 and YM1 were significantly decreased in IFN-β$^{-/-}$ TBI mice. IL-10 production in the CNS is
557 dependent upon IFN-β activity (Lobo-Silva et al. 2017), and inhibition of type I IFN signaling in a
558 model of prion disease reduces IL-10 expression levels (Nazmi et al. 2019). Furthermore, in a
559 respiratory syncytial virus model, YM1 expression in peripheral macrophages also appears to
560 be dependent upon IFN-β (Shirey et al. 2010). Overall, these findings suggest that IFN-β
561 contributes to neuroinflammatory responses by promoting both pro- and anti-inflammatory gene
562 expression.

563 Pro-inflammatory gene expression was also significantly reduced in the hippocampus of
564 IFN-β$^{-/-}$ TBI mice suggesting that IFN-β actively contributes to the propagation of post-traumatic
565 inflammatory responses at distant sites to the primary lesion. Thus, targeted inhibition of IFN-β
566 may limit the spread of damaging inflammatory cascades to other brain regions, thereby
567 reducing functional loss (cognitive deficits). TBI-induced effects on STAT1 and IRF7 were also
568 significantly decreased in the hippocampus of IFNβ$^{-/-}$ mice, along with a significant decrease in
569 viral response genes (ISG15, MX1 and IFI204). Our data suggests that IFN-β upregulates
570 IFI204, which may contribute to detrimental inflammatory processes and functional impairments
571 in the hippocampus through a positive feed-forward induction of type I IFNs (Almine et al. 2017;
572 Storek et al. 2015). Although we demonstrated increased chronic expression of type I IFN
573 related genes at 60 days post-injury, the current study was primarily focused on acute changes
574 including the early transcriptional regulation of type I responses after TBI; future studies will
575 examine chronic mechanisms involved in type I IFN activation, including protein level changes
576 and cell-specific responses.

577 The long-term impact of selectively inhibiting type I IFNs on functional recovery and TBI
578 neuropathology is unknown (Roselli, Chandrasekar, and Morganti-Kossmann 2018). Here, we

demonstrated that IFN-$\beta^{-/-}$ TBI mice had improved long-term motor and cognitive function recovery, which was accompanied by reduced microglial activation and neurodegeneration. We, and others, have shown that NOX2 is a key inflammatory mediator in post-traumatic neurodegeneration, as decreased NOX2 expression is associated with improved neurological function and attenuated neurodegeneration (Kumar et al. 2016; Zhang et al. 2012; Ma et al. 2017; Dohi et al. 2010). In the present study, we show that NOX2 expression in microglia was significantly reduced in IFN-$\beta^{-/-}$ mice compared to WT mice, suggesting that neuroprotection conferred by IFN-$\beta^{-/-}$ is mediated in part through reduced chronic microglial activation. IFNAR1 knockout mice also have improvements in motor function recovery through 7 days post-TBI (Karve et al. 2016) due to loss of IFNAR signaling. Our neurobehavioral analysis through 28 days post-injury demonstrated sustained improvements in motor function in injured IFN-$\beta^{-/-}$ mice. Whereas previous work reported that inhibition of type I IFN signaling can improve cognitive function in normal aging (Baruch et al. 2014) and in AD models (Minter et al. 2016), our study is the first to demonstrate the long-term beneficial effects of IFN-β inhibition on cognitive function after TBI.

To evaluate the translational potential of our genetic studies, we treated TBI mice with a type I IFN neutralizing antibody, αIFNAR. Central administration of αIFNAR initiated at 30 minutes post-injury and continued for 72 hours improved neurological recovery during the sub-acute phase. Others have shown that αIFNAR treatment reduces the production of IFN-α and IFN-β, as well as decreases the production of IL-1β and IL-6 acutely after TBI (Karve et al. 2016). In our study, we show that αIFNAR treatment leads to improved motor and cognitive function recovery after TBI; however, beneficial effects were not sustained beyond 14 days post-injury, and treatment did not reduce lesion volume at 28 days post-injury. One possible explanation for the non-sustained improvements in functional recovery was that the duration of αIFNAR treatment was too short (0-3 days post-injury), allowing IFN-mediated signaling to be

604 restored. Interestingly, RNA sequencing and pathway analyses indicate that immune responses
605 associated with IFN-α and IFN-β signaling are chronically upregulated in isolated microglia up to
606 90 days post-TBI (Makinde et al. 2019). This suggests that type I IFN-related pathways are
607 active for prolonged periods after TBI, and chronic administration of inhibitors will be required to
608 improve long-term neurological recovery. Indeed, our data demonstrate that type I IFNs and
609 microglial activation genes remain chronically elevated up to 60 days post-injury. It is also
610 possible that central infusion of αIFNAR failed to reduce type I IFN-mediated changes in
611 peripheral immune cells. In fact, previous data suggests that ablation of IFNAR signaling on
612 hematopoietic cells is critical for neuroprotection following TBI (Karve et al. 2016). The use of a
613 constitutive IFN-β knockout mouse model is likely to have impacted peripheral immune
614 responses, and this may have contributed to sustained neuroprotection in our genetic studies.
615 Additional studies will be needed to investigate the functional role of IFN-β, and related type I
616 IFNs, in peripheral immune cells following TBI.

617 In summary, TBI induces a robust neuroinflammatory response that is associated with
618 increased expression of IFN-β and other IFN-related genes. Inhibition of IFN-β reduces post-
619 traumatic neuroinflammation and neurodegeneration resulting in long-term motor and cognitive
620 function recovery. These pre-clinical studies suggest that therapeutic inhibition of type I IFNs,
621 and IFN-β in particular, may limit persistent neuroinflammation and the development of motor
622 and cognitive function deficits following moderate-to-severe TBI.
623

Author contribution Statement

James P. Barrett contributed to study conception and design performed *in vivo* studies, collected data, performed data analysis, and manuscript preparation; Rebecca J. Henry contributed to study design, performed *in vivo* studies, collected data, and manuscript preparation; Kari A. Shirey contributed to experimental design and manuscript preparation; Sarah J. Doran contributed to data collection; Oleg D. Makarevich performed data analysis; Rodney R. Ritzel contributed to data collection; Victoria A. Meadows contributed to data collection; Stefanie N Vogel contributed to experimental design and manuscript preparation; Alan I. Faden contributed to experimental design and manuscript preparation; Bogdan A. Stoica contributed to experimental design and manuscript preparation; David J. Loane contributed to study conception, experimental design and manuscript preparation. All authors read and approved the manuscript prior to submission.

637 **Figure Legends**

638 **Figure 1. Type I Interferon (IFN) response in the injured brain following moderate-level**
639 **controlled cortical impact.** Cortical expression of cGAS and STING protein was assessed by
640 Western immunoblotting (representative blot shown in A) in the ipsilateral cortex sham and TBI
641 mice at 72 h post-injury. TBI increased cortical expression of cGAS (p=0.0023, B) and STING
642 (p=0.023, C) protein compared to sham mice. TBI significantly increased the expression of IFN-
643 β mRNA in the cortex of TBI mice (p=0.006, D). The expression of STAT1 protein was
644 significantly increased in the cortex of TBI mice compared to sham mice (p=0.006, E)
645 (representative blot shown in a). mRNA expression of IRF family members was assessed, TBI
646 significantly increased cortical IRF1 (p=0.002, F), IRF3 (p=0.0002, G), IRF4 (p=0.016, H), IRF5
647 (p=0.0002, I) and IRF7 (p=0.046, J) mRNA expression. Expression of cGAS and STING protein
648 was assessed by western immunoblotting (representative blot shown in K) in the hippocampus
649 of sham and TBI mice at 72 h post-injury. TBI increased expression of cGAS (($t_{(8)}$=3.645,
650 p=0.0065, L) and STING ($t_{(8)}$=2.956, p=0.0182, M) protein compared to sham mice. IFN-β
651 mRNA expression was significantly increased in the hippocampus of TBI mice (t(8)=5.447,
652 p=0.0006, N). The expression of STAT1 protein was significantly increased in the hippocampus
653 of TBI mice compared to sham mice (t(8)=3.134, p=0.014, O). mRNA expression of IRF family
654 members was assessed, TBI significantly increased hippocampal IRF1 (t(8)=9.671, p<0.0001,
655 P), IRF3 (($t_{(8)}$=3.523, p=0.00078, Q), IRF4 ($t_{(8)}$=8.455, p<0.0001, R) IRF5 (t(8)=11.92, p<0.0001,
656 S) and IRF7 (t(8)=3.921, p=0.0044, T) mRNA expression. Data expressed as Mean ± SEM
657 (n=5/group). *p<0.05, **p<0.01, ***p<0.001, Student's t test.
658
659 **Figure 2 Type I IFN response following TBI is reduced in IFN-β$^{-/-}$ mice.** Cortical expression
660 of cGAS and STING protein was asessed by Western immunoblotting (representative blot
661 shown in a) in the ipsilateral cortex WT and IFN-β$^{-/-}$sham and TBI mice at 72 h post-injury. TBI
662 significantly increased cortical expression of cGAS (p<0.0001, B) and STING (p<0.0001, C)

protein in WT and IFN-$\beta^{-/-}$ mice. The expression of STAT1 protein was significantly increased in the cortex of TBI mice compared to sham mice (p=0.0004, D), this TBI effect was significantly reduced in IFN-$\beta^{-/-}$ mice (p=0.015, WT TBI vs IFN-$\beta^{-/-}$ TBI). TBI significantly increased mRNA expression of IRF1 (p<0.0001, F), IRF3 (p=0.0478, E), IRF4 (p=0.0208, G), IRF5 (p<0.0001, H) and IRF7 (p<0.0001, I) in WT and IFN-$\beta^{-/-}$ mice. The TBI-induced increase in IRF1 and IRF7 was significantly reduced in IFN-$\beta^{-/-}$ mice (IRF1 [p=0.0016] and IRF7 [p<0.0001], WT TBI vs IFN-$\beta^{-/-}$ TBI). TBI significantly increased the expression of the viral response genes ISG15 (p=0.0005, J), MX1 (p<0.0001, K) and IFI204 (p<0.0001, L) in WT and IFN-$\beta^{-/-}$ mice. This TBI effect was significantly reduced in IFN-$\beta^{-/-}$ mice, ISG15 (p<0.0001, WT TBI vs IFN$^{-/-}$ TBI), MX1 (p<0.0001, WT TBI vs I IFN-$\beta^{-/-}$ TBI) and IFI204 (p<0.0001, WT TBI vs IFN-$\beta^{-/-}$ TBI). Expression of cGAS (l) and STING (m) protein was assessed by western immunoblotting (representative blot shown in j) in ipsilateral hippocampal sham and TBI mice at 72 h post-injury. TBI increased expression of cGAS (p<0.0001, N) and STING (p<0.0001, O) protein compared to sham mice, this TBI effect was significantly reduced in IFN-$\beta^{-/-}$ mice (cGAS [p=0.0007, WT TBI vs IFN-$\beta^{-/-}$ TBI] and STING [p=0.0004, WT TBI vs IFN-$\beta^{-/-}$ TBI]). The expression of STAT1 protein was significantly increased in the hippocampus of TBI mice compared to sham mice (p=0.0014, P), the expression of STAT1 was significantly attenuated in IFN-$\beta^{-/-}$ TBI mice compared to WT TBI mice (p=0.0073). TBI significantly increased hippocampal IRF7 (p=0.0015, Q), ISG15 (p=0.0034, R), MX1 (p=0.0001, S) and IFI204 (p=0.0052, T) mRNA expression. The TBI effect on all of these genes was significantly reduced in IFN-$\beta^{-/-}$ mice, IRF7 (p=0.0002, WT TBI vs IFN-$\beta^{-/-}$ TBI), ISG15 (p=0.0006, WT TBI vs IFN-$\beta^{-/-}$ TBI), MX1 (p<0.0001, WT TBI vs IFN-$\beta^{-/-}$ TBI) and IFI204 (p=0.0078, WT TBI vs IFN-$\beta^{-/-}$ TBI). Data expressed as Mean ± SEM. *p<0.05, **p<0.01, ***p<0.001 vs. sham (effect of TBI) and $^{+}$p<0.05, $^{++}$p<0.01, $^{+++}$p<0.001 WT TBI vs IFN-$\beta^{-/-}$ TBI. Two-way ANOVA, (n=6/group).

Figure 3 IFNβ deficiency reduces the pro-inflammatory response following TBI. Cortical expression of a number of pro-inflammatory genes was assessed in sham and TBI at 72 h post-injury. TBI significantly increased cortical mRNA expression of TNFα ($p<0.0001$, A), NOX2 ($p<0.0001$, B), IL-6 (, $p=0.0014$, C), IL-1β ($p<0.0001$, D), CCL5 ($p<0.0001$, E), CXCL10 ($p<0.0001$, F), ITGAM ($p<0.0001$, G) and GFAP ($p<0.0001$, H) in WT and IFN-$\beta^{-/-}$ mice. The TBI-induced increase in TNFα, NOX2, CCL5 and CXCL10 was significantly reduced in IFN-$\beta^{-/-}$ mice (TNF [$p=0.0131$], NOX2 [$p=0.0027$], CCL5 [$p<0.0001$] and CXCL10 [$p<0.0001$], WT TBI vs IFN-$\beta^{-/-}$ TBI). Hippocampal mRNA expression of TNF, NOX2, CCL5 and CXCL10 was measured in sham and TBI mice at 72 h post-injury. TBI significantly increased hippocampal mRNA expression of TNFα ($F_{(1,16)}=9.745$, $p=0.066$, I), NOX2 ($F_{(1,16)}=11.33$, $p=0.0039$, J), CCL5 ($F_{(1,19)}=15.08$, $p=0.0013$, K) and CXCL10 ($F_{(1,19)}=22.82$, $p=0.0002$, L) in WT and IFN-$\beta^{-/-}$ mice. There was a genotype effect on these genes (NOX2 [$F_{(1,16)}=4.975$, $p=0.0404$], CCL5 [$F_{(1,16)}=5.200$, $p=0.0366$] and CXCL10 [$F_{(1,16)}=20.79$, $p=0.0003$]), and a significant interaction between TBI and genotype (NOX2 [$F_{(1,16)}=5.736$, $p=0.0292$], CCL5 [$F_{(1,16)}=5.839$, $p=0.0280$] and CXCL10 [$F_{(1,16)}=18.94$, $p=0.0005$]). The expression of all genes was significantly reduced in IFN-$\beta^{-/-}$ TBI mice compared to WT TBI mice ((TNFα $p=0.0458$], NOX2 [$p=0.0224$], CCL5 [$p=0.0203$] and CXCL10 [$p<0.0001$], WT TBI vs IFN-$\beta^{-/-}$ TBI). Data expressed as Mean ± SEM. $^{**}p<0.01$, $^{***}p<0.001$ vs. sham (effect of TBI) and $^{+}p<0.05$, $^{++}p<0.01$, $^{+++}p<0.001$ WT TBI vs IFN-$\beta^{-/-}$ TBI. Two-way ANOVA, (n=6/group).

Figure 4 IFN-β deficiency alters the inflammatory response after TBI. Cortical mRNA expression of Arg1, YM1, IL-10, SOCS3 and TGFβ was assessed in WT and IFN-$\beta^{-/-}$ sham and TBI mice. TBI significantly increased cortical mRNA expression of Arg1 ($p=0.0002$, A), YM1 ($p<0.0001$, B), IL-10 ($p<0.0001$, C), SOCS3 ($p<0.0001$, D) and TGFβ ($p<0.0001$, E) in WT and IFN-$\beta^{-/-}$ mice. The effect of TBI on YM1 ($p=0.0022$, WT TBI vs IFN-$\beta^{-/-}$ TBI) and IL-10 ($p<0.0001$,

WT TBI vs IFN-$\beta^{-/-}$ TBI) was significantly reduced in IFN-$\beta^{-/-}$ TBI mice compared to WT TBI mice. Hippocampal mRNA expression of Arg1, YM1, SOCS3 and TGFβ was assessed in WT and IFN-$\beta^{-/-}$ Sham and TBI mice. TBI significantly increased hippocampal mRNA expression of Arg1 ($F_{(1,16)}$=11.70, p=0.0035, F), YM1 ($F_{(1,16)}$=6.131, p=0.0248, G), SOCS3 ($F_{(1,16)}$=9.001, p=0.0085, H) and TGFβ ($F_{(1,16)}$=28.69, p<0.0001, I) in WT and IFN-$\beta^{-/-}$ mice. There was a genotype effect on YM1 ($F_{(1,16)}$=4.737, p=0.0449) and SOCS3 ($F_{(1,16)}$=4.907, p=0.0416), as well as a significant interaction between TBI and genotype for YM1 ($F_{(1,16)}$=4.578, p=0.0481) and SOCS3 ($F_{(1,16)}$=5.153, p=0.0374). Post-hoc analysis demonstrated decreased YM1 and SOCS3 expression in IFN-$\beta^{-/-}$ TBI mice (YM1 [p=0.0345] and SOCS3 [p=0.0273], WT TBI vs IFN-$\beta^{-/-}$ TBI). Data expressed as Mean ± SEM. *p<0.05, **p<0.01, ***p<0.001 vs. sham (effect of TBI) and $^{+}$p<0.05, $^{++}$p<0.01, $^{+++}$p<0.001 WT TBI vs IFN-$\beta^{-/-}$ TBI. Two-way ANOVA, (n=6/group).

Figure 5 IFN-β deficiency improves motor and cognitive function recovery after TBI. Beam walk analysis of sham and TBI WT and IFN-$\beta^{-/-}$ mice. In WT mice TBI induced persistent deficits in fine motor coordination through 28 days post-injury (dpi) (p<0.0001, sham vs. TBI, A). In contrast, IFN-$\beta^{-/-}$ TBI mice had significantly reduced fine motor coordination deficits at 14 dpi, 21 dpi, and 28 dpi (p<0.0001, WT TBI vs. IFN-$\beta^{-/-}$ TBI). TBI induces a significant decrease in the % spontaneous alterations in the Y maze task in WT TBI mice when compared to WT sham counterparts (p=0.0134, B), at 8 dpi. In addition, there was no significant differences between groups in the number of entries in each arm of the Y maze task. In order to assess non-spatial hippocampal-mediated memory, the NOR task was carried out at 18 dpi. TBI mice exhibited a significant decrease in % time spent with the novel object, when compared to sham counterparts (p=0.0008, C). However, the % time IFN-$\beta^{-/-}$ TBI mice spent with the novel object was comparable to sham animals and spent a significant more % of time with the novel object compared to WT TBI mice (p<0.0001). Data expressed as Mean ± SEM. * p < 0.05, ***p<0.001

738 vs. sham (effect of TBI) and $^{+++}$p<0.001 WT TBI vs IFN-β$^{-/-}$ TBI. (A) Two-way repeated measures
739 ANOVA (n=8-13/group) and (B,C) Two-way ANOVA (n=8-13/group).
740
741 **Figure 6 IFN-β deficiency reduces lesion volume and hippocampal neurodegeneration**
742 **after TBI.** Immunofluorescence analysis of NOX2 (green) and CD68 (red) demonstrates that
743 injury-induced NOX2 expression in reactive microglia/macrophages was significantly decreased
744 in IFN-β$^{-/-}$ TBI mice compared to WT TBI mice at 28 dpi (A). Scale bar = 50 μm. Representative
745 images of cresyl violet stained coronal sections from WT and IFN-β$^{-/-}$ TBI mice at 28 dpi (B).
746 Quantification of lesion volume in WT and IFN-β$^{-/-}$ TBI mice at 28 dpi. IFN-β$^{-/-}$ resulted in a
747 significant reduction in TBI lesion volume (p=0.003, A). Quantification of hippocampal
748 neurodegeneration in WT and IFN-β$^{-/-}$ TBI mice at 28 dpi (B). In WT mice TBI resulted in
749 significant loss of hippocampal neurons when compared to the WT sham group. In contrast, TBI
750 in IFN-β$^{-/-}$ mice resulted in reduced neuronal loss, which was significantly different to the WT TBI
751 group. Data expressed as Mean ± SEM. * p < 0.05, ***p<0.001 vs. sham (effect of TBI) and
752 $^{+++}$p<0.001 WT TBI vs IFN-β$^{-/-}$ TBI. (A) Two-way ANOVA (n=4-5/group) (B) Student's t test (n=6-
753 7/group), and (C) Two-way ANOVA (n=4-5/group).
754
755 **Figure 7 Early post-injury inhibition of type I IFN signaling provides transient**
756 **improvements in neurological function following TBI that are lost at later time points.**
757 Beam walk analysis of sham, IgG- and αIFNAR-treated TBI mice at 28 dpi. TBI induced
758 persistent deficits in fine motor coordination in IgG- and αIFNAR-treated TBI mice through 28
759 dpi (p<0.0001, vs. Sham; A). TBI induces a significant decrease in the % spontaneous
760 alterations in the Y maze task in IgG-treated TBI mice when compared to sham counterparts
761 (p=0.0281, vs Sham; B), at 8 dpi. No injury effect was observed in αIFNAR-treated TBI mice, in
762 addition to this, αIFNAR-treated TBI mice exhibited a significant improvement in performance
763 when compared to IgG-treated TBI mice (p=0.0331 vs IgG-treated TBI mice). No significant

differences were observed between groups in the number of entries in each arm of the Y maze task. In order to assess non-spatial hippocampal-mediated memory, the NOR task was carried out at 18 dpi. TBI induced a significant decrease in % time IgG-treated- and αIFNAR-treated TBI mice spent with the novel object, when compared to sham counterparts (TBI+IgG [$p<0.0001$] and TBI+αIFNAR [$p=0.0002$], vs Sham; C). There was no effect of treatment. Representative images for lesion volume in IgG-treated- and αIFNAR-treated TBI mice at 28 dpi. Stereological analysis revealed lesion volume to be similar in IgG-treated- and αIFNAR-treated mice. Data expressed as Mean ± SEM. $^{**}p<0.01$, $^{***}p<0.001$ vs. Sham (effect of TBI) and $^{+++}p<0.001$ TBI + IgG vs TBI+IFNAR. (a) Two-way ANOVA (n=5-9/group), (b,c) One-way ANOVA (n=5-9/group) and (d) Student's t test, (n=8/9group).

Figure 8 Type I IFN genes are chronically elevated in the injured cortex following TBI. Cortical mRNA expression of Type I IFN related genes was assessed at 60 days post-injury. While there was no effect of TBI on cGAS gene expression (A), TBI significantly increased cortical STING ($p=0.0006$, B), STAT1 ($p=0.0020$, C), IRF1 ($p=0.0077$, D), IRF7 ($p=0.046$, E), CXCL10 ($p=0.0074$, E), ISG15 ($p=0.0225$, E) and IFI204 ($p=0.0002$, J) mRNA expression. Chronic TBI also increased mRNA expression of TNFα ($p=0.0101$, I), NOX2 ($p=0.0005$, J), CCL5 ($p=0.003$, K), CD11b ($p<0.0001$, L), CD68 ($p=0.0001$, M), and GFAP ($p=0.0001$, N). Data expressed as Mean ± SEM (n=7/group). $^{*}p<0.05$, $^{**}p<0.01$, $^{***}p<0.001$, Student's t test.

References:

Abdullah, A., M. Zhang, T. Frugier, S. Bedoui, J. M. Taylor, and P. J. Crack. 2018. 'STING-mediated type-I interferons contribute to the neuroinflammatory process and detrimental effects following traumatic brain injury', *J Neuroinflammation*, 15: 323.

Ahyi, A. N., H. C. Chang, A. L. Dent, S. L. Nutt, and M. H. Kaplan. 2009. 'IFN regulatory factor 4 regulates the expression of a subset of Th2 cytokines', *J Immunol*, 183: 1598-606.

Akira, S., S. Uematsu, and O. Takeuchi. 2006. 'Pathogen recognition and innate immunity', *Cell*, 124: 783-801.

Almine, J. F., C. A. O'Hare, G. Dunphy, I. R. Haga, R. J. Naik, A. Atrih, D. J. Connolly, J. Taylor, I. R. Kelsall, A. G. Bowie, P. M. Beard, and L. Unterholzner. 2017. 'IFI16 and cGAS cooperate in the activation of STING during DNA sensing in human keratinocytes', *Nat Commun*, 8: 14392.

Aungst, S. L., S. V. Kabadi, S. M. Thompson, B. A. Stoica, and A. I. Faden. 2014. 'Repeated mild traumatic brain injury causes chronic neuroinflammation, changes in hippocampal synaptic plasticity, and associated cognitive deficits', *J Cereb Blood Flow Metab*, 34: 1223-32.

Barrett, J. P., R. J. Henry, S. Villapol, B. A. Stoica, A. Kumar, M. P. Burns, A. I. Faden, and D. J. Loane. 2017. 'NOX2 deficiency alters macrophage phenotype through an IL-10/STAT3 dependent mechanism: implications for traumatic brain injury', *J Neuroinflammation*, 14: 65.

Baruch, K., A. Deczkowska, E. David, J. M. Castellano, O. Miller, A. Kertser, T. Berkutzki, Z. Barnett-Itzhaki, D. Bezalel, T. Wyss-Coray, I. Amit, and M. Schwartz. 2014. 'Aging. Aging-induced type I interferon response at the choroid plexus negatively affects brain function', *Science*, 346: 89-93.

Byrnes, A. A., J. C. McArthur, and C. L. Karp. 2002. 'Interferon-beta therapy for multiple sclerosis induces reciprocal changes in interleukin-12 and interleukin-10 production', *Ann Neurol*, 51: 165-74.

Byrnes, K. R., D. J. Loane, B. A. Stoica, J. Zhang, and A. I. Faden. 2012. 'Delayed mGluR5 activation limits neuroinflammation and neurodegeneration after traumatic brain injury', *J Neuroinflammation*, 9: 43.

Cheng, W. Y., X. B. He, H. J. Jia, G. H. Chen, Q. W. Jin, Z. L. Long, and Z. Z. Jing. 2018. 'The cGas-Sting Signaling Pathway Is Required for the Innate Immune Response Against Ectromelia Virus', *Front Immunol*, 9: 1297.

Chin, A. C. 2019. 'Neuroinflammation and the cGAS-STING pathway', *J Neurophysiol*, 121: 1087-91.

Cox, D. J., R. H. Field, D. G. Williams, M. Baran, A. G. Bowie, C. Cunningham, and A. Dunne. 2015. 'DNA sensors are expressed in astrocytes and microglia in vitro and are upregulated during gliosis in neurodegenerative disease', *Glia*, 63: 812-25.

Deonarain, R., A. Verma, A. C. Porter, D. R. Gewert, L. C. Platanias, and E. N. Fish. 2003. 'Critical roles for IFN-beta in lymphoid development, myelopoiesis, and tumor development: links to tumor necrosis factor alpha', *Proc Natl Acad Sci U S A*, 100: 13453-8.

Dixon, C. E., P. M. Kochanek, H. Q. Yan, J. K. Schiding, R. G. Griffith, E. Baum, D. W. Marion, and S. T. DeKosky. 1999. 'One-year study of spatial memory performance, brain morphology, and cholinergic markers after moderate controlled cortical impact in rats', *J Neurotrauma*, 16: 109-22.

Dohi, K., H. Ohtaki, T. Nakamachi, S. Yofu, K. Satoh, K. Miyamoto, D. Song, S. Tsunawaki, S. Shioda, and T. Aruga. 2010. 'Gp91phox (NOX2) in classically activated microglia exacerbates traumatic brain injury', *J Neuroinflammation*, 7: 41.

Field, R., S. Campion, C. Warren, C. Murray, and C. Cunningham. 2010. 'Systemic challenge with the TLR3 agonist poly I:C induces amplified IFNalpha/beta and IL-1beta responses in the diseased brain and exacerbates chronic neurodegeneration', *Brain Behav Immun*, 24: 996-1007.

Gok, B., O. Okutan, E. Beskonakli, S. Palaoglu, H. Erdamar, and M. F. Sargon. 2007. 'Effect of immunomodulation with human interferon-beta on early functional recovery from experimental spinal cord injury', *Spine (Phila Pa 1976)*, 32: 873-80.

Gunthner, R., and H. J. Anders. 2013. 'Interferon-regulatory factors determine macrophage phenotype polarization', *Mediators Inflamm*, 2013: 731023.

Hatesuer, B., H. T. Hoang, P. Riese, S. Trittel, I. Gerhauser, H. Elbahesh, R. Geffers, E. Wilk, and K. Schughart. 2017. 'Deletion of Irf3 and Irf7 Genes in Mice Results in Altered Interferon Pathway Activation and Granulocyte-Dominated Inflammatory Responses to Influenza A Infection', *J Innate Immun*, 9: 145-61.

Henry, R. J., S. J. Doran, J. P. Barrett, V. E. Meadows, B. Sabirzhanov, B. A. Stoica, D. J. Loane, and A. I. Faden. 2019. 'Inhibition of miR-155 Limits Neuroinflammation and Improves Functional Recovery After Experimental Traumatic Brain Injury in Mice', *Neurotherapeutics*, 16: 216-30.

Honda, K., A. Takaoka, and T. Taniguchi. 2006. 'Type I interferon [corrected] gene induction by the interferon regulatory factor family of transcription factors', *Immunity*, 25: 349-60.

Honda, K., and T. Taniguchi. 2006. 'IRFs: master regulators of signalling by Toll-like receptors and cytosolic pattern-recognition receptors', *Nat Rev Immunol*, 6: 644-58.

Honda, K., H. Yanai, H. Negishi, M. Asagiri, M. Sato, T. Mizutani, N. Shimada, Y. Ohba, A. Takaoka, N. Yoshida, and T. Taniguchi. 2005. 'IRF-7 is the master regulator of type-I interferon-dependent immune responses', *Nature*, 434: 772-7.

Ivashkiv, L. B., and L. T. Donlin. 2014. 'Regulation of type I interferon responses', *Nat Rev Immunol*, 14: 36-49.

Jacobs, L. D., R. W. Beck, J. H. Simon, R. P. Kinkel, C. M. Brownscheidle, T. J. Murray, N. A. Simonian, P. J. Slasor, and A. W. Sandrock. 2000. 'Intramuscular interferon beta-1a therapy initiated during a first demyelinating event in multiple sclerosis. CHAMPS Study Group', *N Engl J Med*, 343: 898-904.

Johnson, V. E., J. E. Stewart, F. D. Begbie, J. Q. Trojanowski, D. H. Smith, and W. Stewart. 2013. 'Inflammation and white matter degeneration persist for years after a single traumatic brain injury', *Brain*, 136: 28-42.

Karve, I. P., M. Zhang, M. Habgood, T. Frugier, K. M. Brody, M. Sashindranath, C. J. Ek, S. Chappaz, B. T. Kile, D. Wright, H. Wang, L. Johnston, M. Daglas, R. C. Ates, R. L. Medcalf, J. M. Taylor, and P. J. Crack. 2016. 'Ablation of Type-1 IFN

876 Signaling in Hematopoietic Cells Confers Protection Following Traumatic Brain
877 Injury', *eNeuro*, 3.
878 Kumar, A., J. P. Barrett, D. M. Alvarez-Croda, B. A. Stoica, A. I. Faden, and D. J.
879 Loane. 2016. 'NOX2 drives M1-like microglial/macrophage activation and
880 neurodegeneration following experimental traumatic brain injury', *Brain Behav*
881 *Immun*, 58: 291-309.
882 Kumar, A., B. A. Stoica, B. Sabirzhanov, M. P. Burns, A. I. Faden, and D. J. Loane.
883 2013. 'Traumatic brain injury in aged animals increases lesion size and
884 chronically alters microglial/macrophage classical and alternative activation
885 states', *Neurobiol Aging*, 34: 1397-411.
886 Lazear, H. M., A. Lancaster, C. Wilkins, M. S. Suthar, A. Huang, S. C. Vick, L. Clepper,
887 L. Thackray, M. M. Brassil, H. W. Virgin, J. Nikolich-Zugich, A. V. Moses, M.
888 Gale, Jr., K. Fruh, and M. S. Diamond. 2013. 'IRF-3, IRF-5, and IRF-7
889 coordinately regulate the type I IFN response in myeloid dendritic cells
890 downstream of MAVS signaling', *PLoS Pathog*, 9: e1003118.
891 Liu, J., S. Cao, L. M. Herman, and X. Ma. 2003. 'Differential regulation of interleukin
892 (IL)-12 p35 and p40 gene expression and interferon (IFN)-gamma-primed IL-12
893 production by IFN regulatory factor 1', *J Exp Med*, 198: 1265-76.
894 Livak, K. J., and T. D. Schmittgen. 2001. 'Analysis of relative gene expression data
895 using real-time quantitative PCR and the 2(-Delta Delta C(T)) Method', *Methods*,
896 25: 402-8.
897 Loane, D. J., A. Kumar, B. A. Stoica, R. Cabatbat, and A. I. Faden. 2014. 'Progressive
898 neurodegeneration after experimental brain trauma: association with chronic
899 microglial activation', *J Neuropathol Exp Neurol*, 73: 14-29.
900 Loane, D. J., A. Pocivavsek, C. E. Moussa, R. Thompson, Y. Matsuoka, A. I. Faden, G.
901 W. Rebeck, and M. P. Burns. 2009. 'Amyloid precursor protein secretases as
902 therapeutic targets for traumatic brain injury', *Nat Med*, 15: 377-9.
903 Lobo-Silva, D., G. M. Carriche, A. G. Castro, S. Roque, and M. Saraiva. 2017.
904 'Interferon-beta regulates the production of IL-10 by toll-like receptor-activated
905 microglia', *Glia*, 65: 1439-51.
906 Ma, M. W., J. Wang, K. M. Dhandapani, and D. W. Brann. 2017. 'NADPH Oxidase 2
907 Regulates NLRP3 Inflammasome Activation in the Brain after Traumatic Brain
908 Injury', *Oxid Med Cell Longev*, 2017: 6057609.
909 Maas, A. I. R., D. K. Menon, P. D. Adelson, N. Andelic, M. J. Bell, A. Belli, P. Bragge, A.
910 Brazinova, A. Buki, R. M. Chesnut, G. Citerio, M. Coburn, D. J. Cooper, A. T.
911 Crowder, E. Czeiter, M. Czosnyka, R. Diaz-Arrastia, J. P. Dreier, A. C. Duhaime,
912 A. Ercole, T. A. van Essen, V. L. Feigin, G. Gao, J. Giacino, L. E. Gonzalez-Lara,
913 R. L. Gruen, D. Gupta, J. A. Hartings, S. Hill, J. Y. Jiang, N. Ketharanathan, E. J.
914 O. Kompanje, L. Lanyon, S. Laureys, F. Lecky, H. Levin, H. F. Lingsma, M.
915 Maegele, M. Majdan, G. Manley, J. Marsteller, L. Mascia, C. McFadyen, S.
916 Mondello, V. Newcombe, A. Palotie, P. M. Parizel, W. Peul, J. Piercy, S.
917 Polinder, L. Puybasset, T. E. Rasmussen, R. Rossaint, P. Smielewski, J.
918 Soderberg, S. J. Stanworth, M. B. Stein, N. von Steinbuchel, W. Stewart, E. W.
919 Steyerberg, N. Stocchetti, A. Synnot, B. Te Ao, O. Tenovuo, A. Theadom, D.
920 Tibboel, W. Videtta, K. K. W. Wang, W. H. Williams, L. Wilson, K. Yaffe, Tbir
921 Participants In, and Investigators. 2017. 'Traumatic brain injury: integrated

approaches to improve prevention, clinical care, and research', *Lancet Neurol*, 16: 987-1048.

Main, B. S., M. Zhang, K. M. Brody, S. Ayton, T. Frugier, D. Steer, D. Finkelstein, P. J. Crack, and J. M. Taylor. 2016. 'Type-1 interferons contribute to the neuroinflammatory response and disease progression of the MPTP mouse model of Parkinson's disease', *Glia*, 64: 1590-604.

Makinde, H. M., T. B. Just, G. T. Gadhvi, D. R. Winter, and S. J. Schwulst. 2019. 'Microglia Adopt Longitudinal Transcriptional Changes After Traumatic Brain Injury', *J Surg Res*, 246: 113-22.

Minter, M. R., Z. Moore, M. Zhang, K. M. Brody, N. C. Jones, S. R. Shultz, J. M. Taylor, and P. J. Crack. 2016. 'Deletion of the type-1 interferon receptor in APPSWE/PS1DeltaE9 mice preserves cognitive function and alters glial phenotype', *Acta Neuropathol Commun*, 4: 72.

Mortimer, J. A., L. R. French, J. T. Hutton, and L. M. Schuman. 1985. 'Head injury as a risk factor for Alzheimer's disease', *Neurology*, 35: 264-7.

Mouzon, B. C., C. Bachmeier, A. Ferro, J. O. Ojo, G. Crynen, C. M. Acker, P. Davies, M. Mullan, W. Stewart, and F. Crawford. 2014. 'Chronic neuropathological and neurobehavioral changes in a repetitive mild traumatic brain injury model', *Ann Neurol*, 75: 241-54.

Muller, U., U. Steinhoff, L. F. Reis, S. Hemmi, J. Pavlovic, R. M. Zinkernagel, and M. Aguet. 1994. 'Functional role of type I and type II interferons in antiviral defense', *Science*, 264: 1918-21.

Nazmi, A., R. H. Field, E. W. Griffin, O. Haugh, E. Hennessy, D. Cox, R. Reis, L. Tortorelli, C. L. Murray, A. B. Lopez-Rodriguez, L. Jin, E. C. Lavelle, A. Dunne, and C. Cunningham. 2019. 'Chronic neurodegeneration induces type I interferon synthesis via STING, shaping microglial phenotype and accelerating disease progression', *Glia*, 67: 1254-76.

Owens, T., R. Khorooshi, A. Wlodarczyk, and N. Asgari. 2014. 'Interferons in the central nervous system: a few instruments play many tunes', *Glia*, 62: 339-55.

Paty, D. W., and D. K. Li. 1993. 'Interferon beta-1b is effective in relapsing-remitting multiple sclerosis. II. MRI analysis results of a multicenter, randomized, double-blind, placebo-controlled trial. UBC MS/MRI Study Group and the IFNB Multiple Sclerosis Study Group', *Neurology*, 43: 662-7.

Piao, C. S., B. A. Stoica, J. Wu, B. Sabirzhanov, Z. Zhao, R. Cabatbat, D. J. Loane, and A. I. Faden. 2013. 'Late exercise reduces neuroinflammation and cognitive dysfunction after traumatic brain injury', *Neurobiol Dis*, 54: 252-63.

Pierce, J. E., D. H. Smith, J. Q. Trojanowski, and T. K. McIntosh. 1998. 'Enduring cognitive, neurobehavioral and histopathological changes persist for up to one year following severe experimental brain injury in rats', *Neuroscience*, 87: 359-69.

Pinto, A. K., H. J. Ramos, X. Wu, S. Aggarwal, B. Shrestha, M. Gorman, K. Y. Kim, M. S. Suthar, J. P. Atkinson, M. Gale, Jr., and M. S. Diamond. 2014. 'Deficient IFN signaling by myeloid cells leads to MAVS-dependent virus-induced sepsis', *PLoS Pathog*, 10: e1004086.

Pischiutta, F., E. Micotti, J. R. Hay, I. Marongiu, E. Sammali, D. Tolomeo, G. Vegliante, N. Stocchetti, G. Forloni, M. G. De Simoni, W. Stewart, and E. R. Zanier. 2018.

'Single severe traumatic brain injury produces progressive pathology with ongoing contralateral white matter damage one year after injury', *Exp Neurol*, 300: 167-78.

Plassman, B. L., R. J. Havlik, D. C. Steffens, M. J. Helms, T. N. Newman, D. Drosdick, C. Phillips, B. A. Gau, K. A. Welsh-Bohmer, J. R. Burke, J. M. Guralnik, and J. C. Breitner. 2000. 'Documented head injury in early adulthood and risk of Alzheimer's disease and other dementias', *Neurology*, 55: 1158-66.

Prinz, M., H. Schmidt, A. Mildner, K. P. Knobeloch, U. K. Hanisch, J. Raasch, D. Merkler, C. Detje, I. Gutcher, J. Mages, R. Lang, R. Martin, R. Gold, B. Becher, W. Bruck, and U. Kalinke. 2008. 'Distinct and nonredundant in vivo functions of IFNAR on myeloid cells limit autoimmunity in the central nervous system', *Immunity*, 28: 675-86.

Ramlackhansingh, A. F., D. J. Brooks, R. J. Greenwood, S. K. Bose, F. E. Turkheimer, K. M. Kinnunen, S. Gentleman, R. A. Heckemann, K. Gunanayagam, G. Gelosa, and D. J. Sharp. 2011. 'Inflammation after trauma: microglial activation and traumatic brain injury', *Ann Neurol*, 70: 374-83.

Roselli, F., A. Chandrasekar, and M. C. Morganti-Kossmann. 2018. 'Interferons in Traumatic Brain and Spinal Cord Injury: Current Evidence for Translational Application', *Front Neurol*, 9: 458.

Roy, E. R., B. Wang, Y. W. Wan, G. S. Chiu, A. L. Cole, Z. Yin, N. E. Propson, Y. Xu, J. L. Jankowsky, Z. Liu, V. M. Lee, J. Q. Trojanowski, S. D. Ginsberg, O. Butovsky, H. Zheng, and W. Cao. 2020. 'Type I interferon response drives neuroinflammation and synapse loss in Alzheimer disease', *J Clin Invest*.

Salib, E., and V. Hillier. 1997. 'Head injury and the risk of Alzheimer's disease: a case control study', *Int J Geriatr Psychiatry*, 12: 363-8.

Sandrow-Feinberg, H. R., V. Zhukareva, L. Santi, K. Miller, J. S. Shumsky, D. P. Baker, and J. D. Houle. 2010. 'PEGylated interferon-beta modulates the acute inflammatory response and recovery when combined with forced exercise following cervical spinal contusion injury', *Exp Neurol*, 223: 439-51.

Scheu, S., S. Ali, R. Mann-Nuttel, L. Richter, V. Arolt, U. Dannlowski, T. Kuhlmann, L. Klotz, and J. Alferink. 2019. 'Interferon beta-Mediated Protective Functions of Microglia in Central Nervous System Autoimmunity', *Int J Mol Sci*, 20.

Sen, T., P. Saha, R. Gupta, L. M. Foley, T. Jiang, O. S. Abakumova, T. K. Hitchens, and N. Sen. 2020. 'Aberrant ER Stress Induced Neuronal-IFNbeta Elicits White Matter Injury Due to Microglial Activation and T-Cell Infiltration after TBI', *J Neurosci*, 40: 424-46.

Sheikh, F., H. Dickensheets, A. M. Gamero, S. N. Vogel, and R. P. Donnelly. 2014. 'An essential role for IFN-beta in the induction of IFN-stimulated gene expression by LPS in macrophages', *J Leukoc Biol*, 96: 591-600.

Shirey, K. A., L. M. Pletneva, A. C. Puche, A. D. Keegan, G. A. Prince, J. C. Blanco, and S. N. Vogel. 2010. 'Control of RSV-induced lung injury by alternatively activated macrophages is IL-4R alpha-, TLR4-, and IFN-beta-dependent', *Mucosal Immunol*, 3: 291-300.

Smith, C., S. M. Gentleman, P. D. Leclercq, L. S. Murray, W. S. Griffin, D. I. Graham, and J. A. Nicoll. 2013. 'The neuroinflammatory response in humans after traumatic brain injury', *Neuropathol Appl Neurobiol*, 39: 654-66.

1014 Storek, K. M., N. A. Gertsvolf, M. B. Ohlson, and D. M. Monack. 2015. 'cGAS and Ifi204
1015 cooperate to produce type I IFNs in response to Francisella infection', *J Immunol*,
1016 194: 3236-45.
1017 Takaoka, A., H. Yanai, S. Kondo, G. Duncan, H. Negishi, T. Mizutani, S. Kano, K.
1018 Honda, Y. Ohba, T. W. Mak, and T. Taniguchi. 2005. 'Integral role of IRF-5 in the
1019 gene induction programme activated by Toll-like receptors', *Nature*, 434: 243-9.
1020 Tanaka, T., K. Murakami, Y. Bando, and S. Yoshida. 2015. 'Interferon regulatory factor
1021 7 participates in the M1-like microglial polarization switch', *Glia*, 63: 595-610.
1022 Taylor, J. M., M. R. Minter, A. G. Newman, M. Zhang, P. A. Adlard, and P. J. Crack.
1023 2014. 'Type-1 interferon signaling mediates neuro-inflammatory events in models
1024 of Alzheimer's disease', *Neurobiol Aging*, 35: 1012-23.
1025 Thomas, K. E., C. L. Galligan, R. D. Newman, E. N. Fish, and S. N. Vogel. 2006.
1026 'Contribution of interferon-beta to the murine macrophage response to the toll-like
1027 receptor 4 agonist, lipopolysaccharide', *J Biol Chem*, 281: 31119-30.
1028 Walko, T. D., 3rd, R. A. Bola, J. D. Hong, A. K. Au, M. J. Bell, P. M. Kochanek, R. S.
1029 Clark, and R. K. Aneja. 2014. 'Cerebrospinal fluid mitochondrial DNA: a novel
1030 DAMP in pediatric traumatic brain injury', *Shock*, 41: 499-503.
1031 Wang, H. C., Y. T. Lin, S. Y. Hsu, N. W. Tsai, Y. R. Lai, B. Y. Su, C. T. Kung, and C. H.
1032 Lu. 2019. 'Serial plasma DNA levels as predictors of outcome in patients with
1033 acute traumatic cervical spinal cord injury', *J Transl Med*, 17: 329.
1034 Xie, C., C. Liu, B. Wu, Y. Lin, T. Ma, H. Xiong, Q. Wang, Z. Li, C. Ma, and Z. Tu. 2016.
1035 'Effects of IRF1 and IFN-beta interaction on the M1 polarization of macrophages
1036 and its antitumor function', *Int J Mol Med*, 38: 148-60.
1037 Zhang, Q. G., M. D. Laird, D. Han, K. Nguyen, E. Scott, Y. Dong, K. M. Dhandapani,
1038 and D. W. Brann. 2012. 'Critical role of NADPH oxidase in neuronal oxidative
1039 damage and microglia activation following traumatic brain injury', *PLoS One*, 7:
1040 e34504.
1041

Cortex

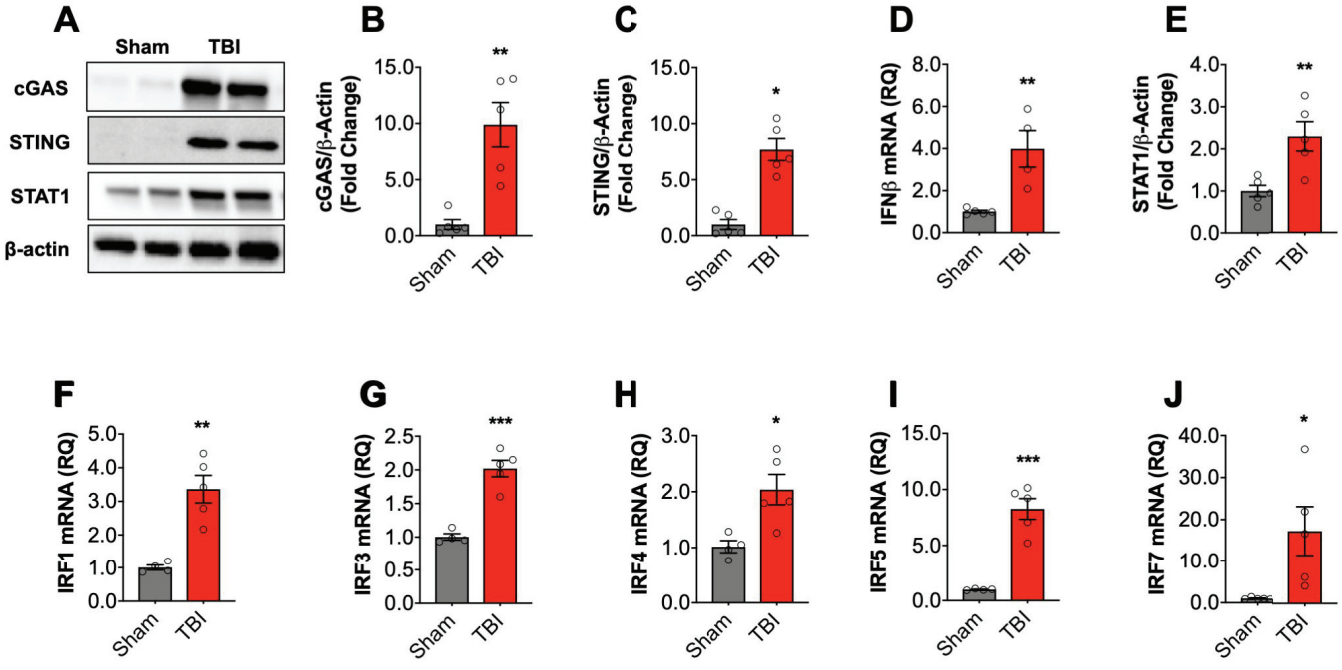

Hippocampus

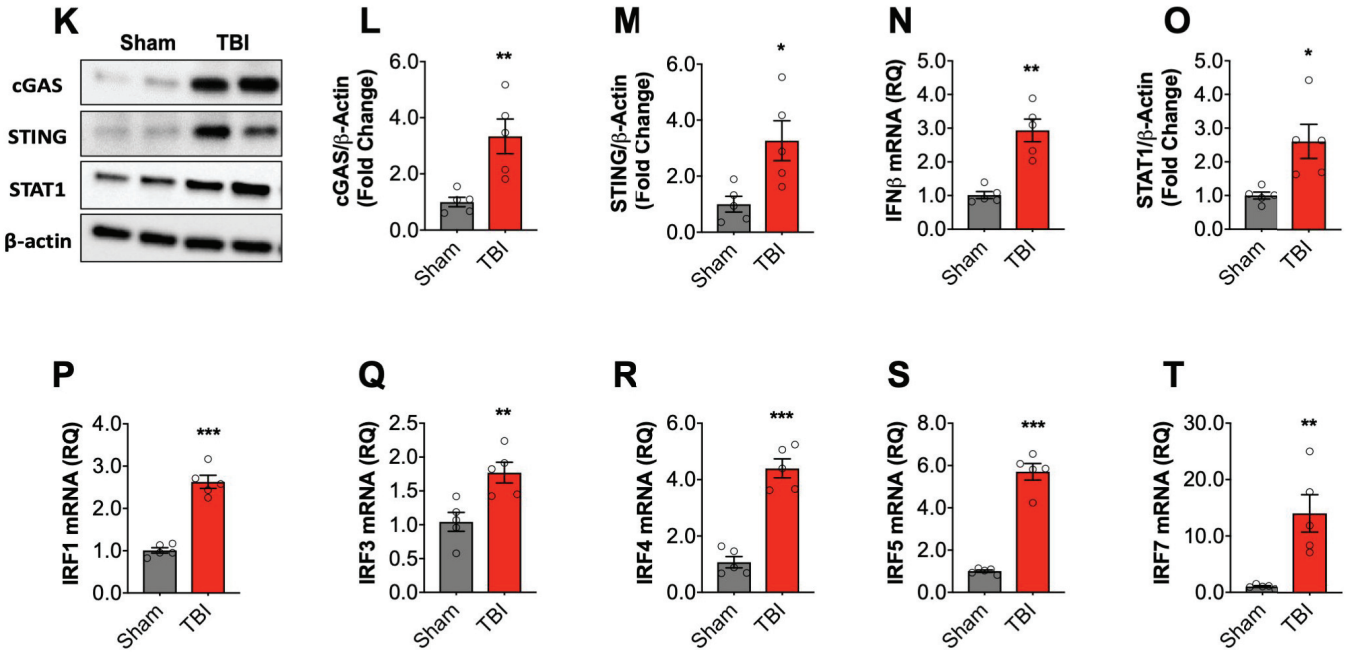

Cortex

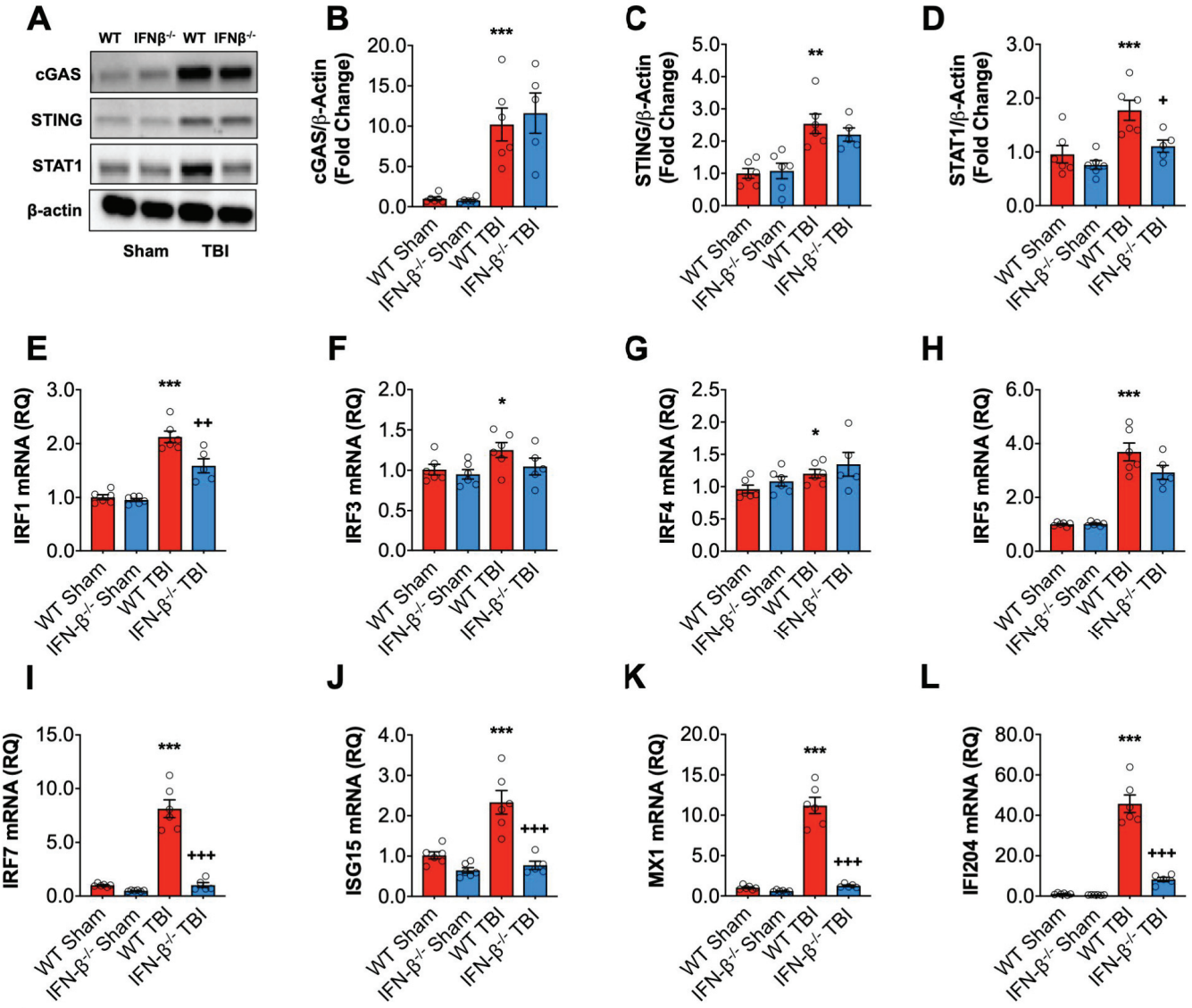

Hippocampus

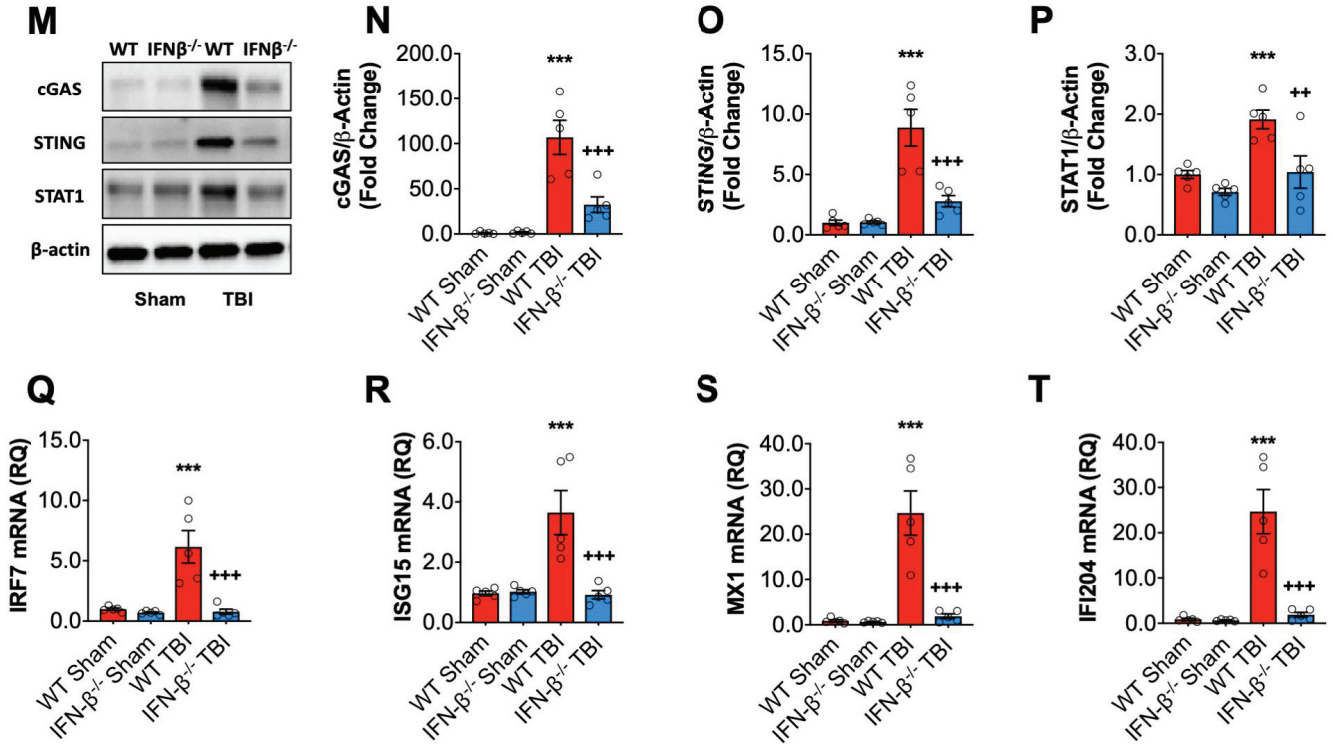

Cortex

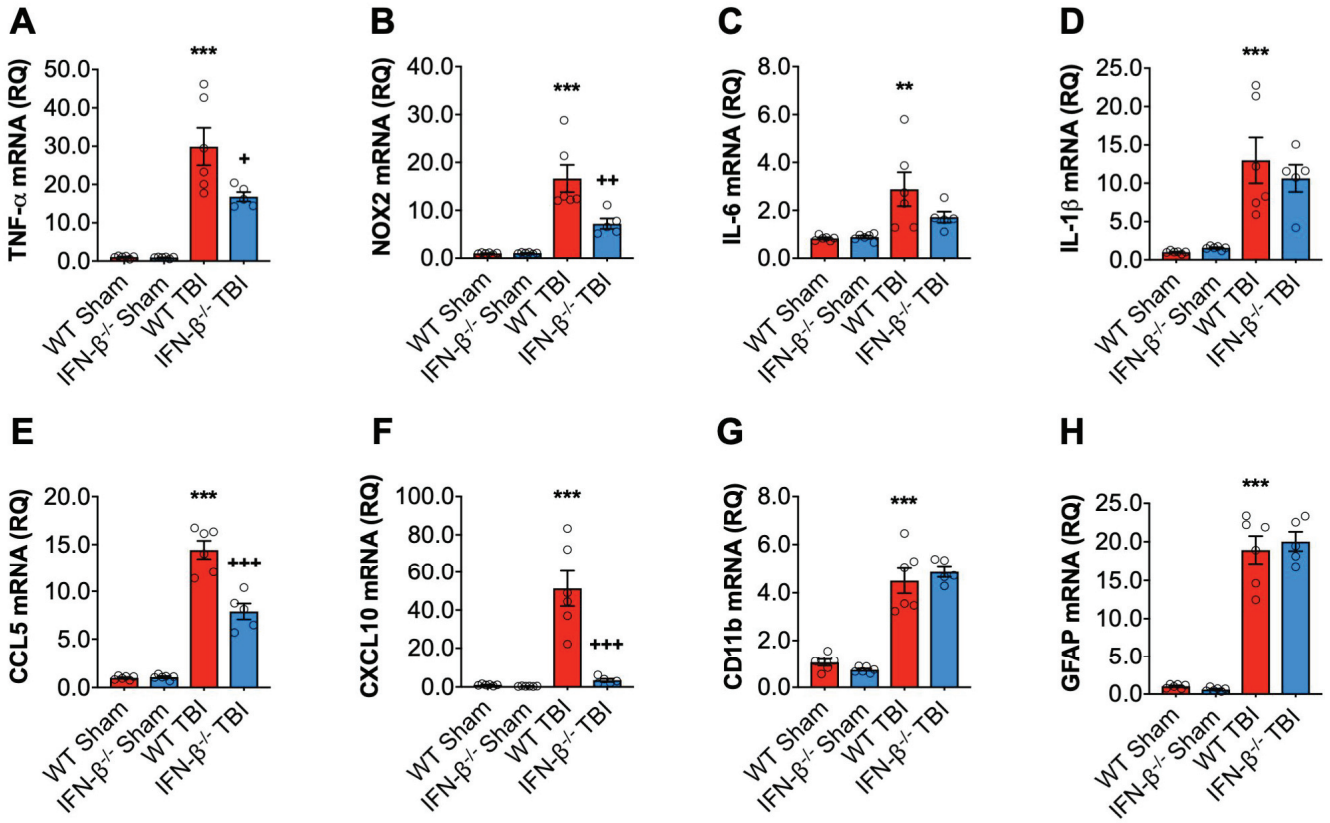

Hippocampus

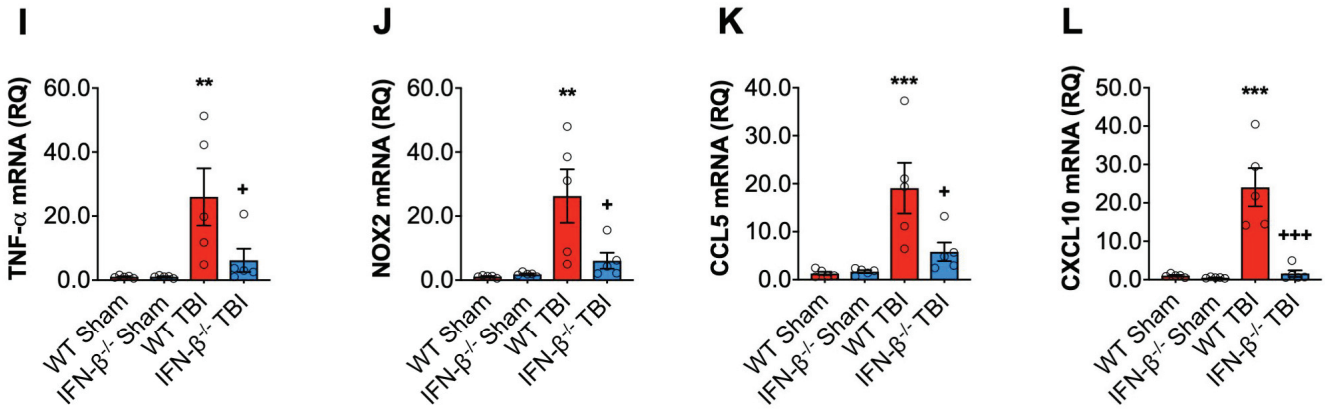

Cortex

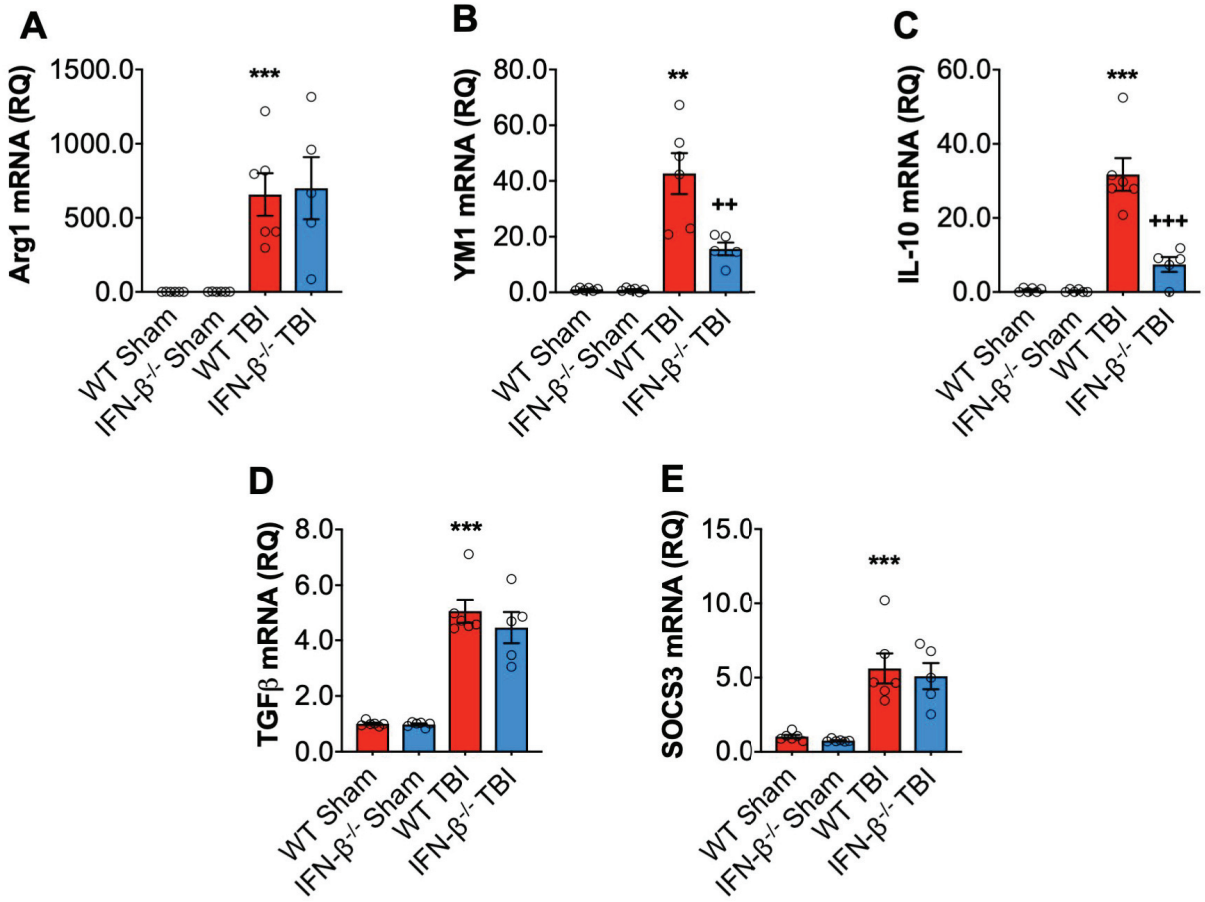

Hippocampus